bioRxiv preprint doi: https://doi.org/10.1101/2023.10.23.563079; this version posted October 25, 2023. The copyright holder for this preprint (which was not certified by peer review) is the author/funder, who has granted bioRxiv a license to display the preprint in perpetuity. It is made available under aCC-BY-NC 4.0 International license.

Dynamic model of carbon dioxide-induced stomatal closure reveals a feedback core for cellular decision-making

Xiao Gan[1,2,3*], Palanivelu Sengottaiyan[3], Kyu Hyong Park[2], Sarah M. Assmann[3*] and Réka Albert[2,3*]

1. Institute for AI in Medicine, School of Artificial Intelligence, Nanjing University of Information Science and Technology, Nanjing 210044, China

2. Department of Physics, Pennsylvania State University, University Park, 16802

3. Department of Biology, Pennsylvania State University, University Park, 16802

* To whom correspondence may be addressed: Dr. Xiao Gan, email: xiao.gan@nuist.edu.cn; Prof. Sarah M. Assmann: sma3@psu.edu; Prof. Réka Albert, email: rza1@psu.edu

Abstract

Stomata are pores on plant aerial surfaces, each bordered by a pair of guard cells. They control gas exchange vital for plant survival. Understanding how guard cells respond to environmental signals such as atmospheric carbon dioxide (CO_2) levels is not only insightful to fundamental biology but also relevant to real-world issues of crop productivity under global climate change. In the past decade, multiple important signaling elements for stomatal closure induced by elevated CO_2 have been identified. Yet, there is no comprehensive understanding of high CO_2 induced stomatal closure. In this work we assemble a cellular signaling network underlying high CO_2-induced stomatal closure by integrating evidence from a comprehensive literature analysis. We further construct a Boolean dynamic model of the network, which allows *in silico* simulation of the stomatal closure response to high CO_2 in wild-type *Arabidopsis thaliana* plants and in cases of pharmacological or genetic manipulation of network nodes. Our model has a 91% accuracy in capturing known experimental observations. We perform network-based logical analysis and reveal a feedback core of the network, which dictates cellular decisions in closure response to high CO_2. Based on these analyses, we predict and experimentally confirm that applying nitric oxide (NO) induces stomatal closure in ambient CO_2 and causes hypersensitivity to elevated CO_2. Moreover, we predict a negative regulatory relationship between NO and the protein phosphatase ABI2 and find experimentally that NO inhibits ABI2 phosphatase activity. The experimental validation of these model predictions demonstrates the effectiveness of network-based modeling and highlights the decision-making role of the feedback core of the network in signal transduction. We further explore the model's potential in predicting targets of signaling elements not yet connected to the CO_2 network. Our combination of network science, *in silico* model simulation, and experimental assays demonstrates an effective interdisciplinary approach to understanding system-level biology.

bioRxiv preprint doi: https://doi.org/10.1101/2023.10.23.563079; this version posted October 25, 2023. The copyright holder for this preprint (which was not certified by peer review) is the author/funder, who has granted bioRxiv a license to display the preprint in perpetuity. It is made available under aCC-BY-NC 4.0 International license.

I. Introduction

Stomata are microscopic pores on plant leaf surfaces that control gas exchange such as the uptake of CO_2, and the release of water vapor and photosynthetically-produced O_2. Each stomate is bordered by two guard cells, whose shape change in response to the external and internal environment controls the stomate's opening or closure. Because plants inevitably lose water via transpiration through the stomata, the size of the stomatal pores is tightly regulated to balance the competing needs of CO_2 supply for photosynthesis and plant hydration. Stomata open in response to environmental signals such as light and low atmospheric CO_2 levels and close in response to darkness, high CO_2, drought, and low humidity [1]. As elucidated in detail for the stress hormone abscisic acid (ABA) [2-4], stimulus perception activates an intracellular signal transduction network, which leads to Ca^{2+} influx and anion efflux, with consequent membrane depolarization promoting K^+ efflux. The outflow of ions increases cellular water potential, creating a driving force for water efflux through aquaporins, which finally causes guard cell deflation and stomatal closure. However, the extent to which the ABA signal transduction network is shared by other closure signals such as darkness and high CO_2 is currently not elucidated [2].

Understanding how stomata respond to high CO_2 is a fundamental question for plant biology. Since stomata control gas exchange vital for plant water retention and photosynthesis, stomatal response to abiotic stress is an essential process for plant survival. Furthermore, understanding plant response to high CO_2 also has imperative practical significance: over the past 60 years, CO_2 concentration in the atmosphere has increased by 32% (NOAA at Mauna Loa [5]). The greenhouse effect induced by increased CO_2 has increased global temperature, which exacerbates drought, compounding the stress. Plant stomatal responses to CO_2 are therefore highly relevant to real-world issues of crop productivity under the adversity posed by climate change.

Current knowledge of high CO_2 signaling in guard cells

Stomatal movement in response to high CO_2 concentration is a complex process in which numerous cellular elements have been implicated by prior studies. These elements interact with and regulate each other via chemical reactions, protein interactions, and physical processes, forming a complex cell signaling network that propagates the signal from CO_2 to stomatal closure. Atmospheric CO_2 enters guard cells through CO_2 porins [6]. The CO_2-binding carbonic anhydrase enzymes CA1 and CA4 catalyze the reversible chemical reaction $CO_2 + H_2O \rightarrow HCO_3^- + H^+$, and these enzymes are a demonstrated component of the CO_2 signal transduction mechanism [7, 8]. HT1 (high leaf temperature 1) is an important CO_2 signaling element that inhibits the activation of the main anion channel SLAC1 (SLOW ANION CHANNEL-ASSOCIATED 1). Multiple mutants of HT1 have been shown to result in insensitivity to high CO_2 [9-11]. Mitogen-activated protein kinases 4 and 12 (MPK4/12) bind to HT1 and inhibit its kinase activity [11, 12]. Bicarbonate enhances and stabilizes the binding of MPK4/12 to HT1 [13, 14]. Arabidopsis RESISTANT TO HIGH CO_2 (RHC1), a MATE-type transporter, may also link elevated CO_2 concentration to repression of

bioRxiv preprint doi: https://doi.org/10.1101/2023.10.23.563079; this version posted October 25, 2023. The copyright holder for this preprint (which was not certified by peer review) is the author/funder, who has granted bioRxiv a license to display the preprint in perpetuity. It is made available under aCC-BY-NC 4.0 International license.

HT1, although this has been debated [15, 16]. Disruption of the second messengers Ca^{2+}_{cyt}, ROS (reactive oxygen species), or NO (nitric oxide) impairs high CO_2 induced closure [17-22], implicating them in CO_2 signaling. Despite the recent identification of key elements and pathways in the high CO_2 response, further elucidation is needed of how the known elements and pathways interact with each other to induce stomatal closure. A systems biology approach integrating existing evidence into a signaling network can identify the gaps of knowledge and suggest potential ways to elucidate all the mechanisms that contribute to stomatal closure.

Prior modeling of guard cell signaling networks

In the past, our team has developed multiple networks and network-based models to characterize the guard cell signaling system. In 2006, Li et al. constructed a Boolean model of ABA (abscisic acid)-induced stomatal closure [23]. In 2014, Sun et al. developed a multi-level discrete dynamic model focusing on light-induced stomatal opening [24]. In 2017, Albert et al. made major updates to the ABA-induced stomatal closure model, including many more signaling elements discovered in recent years [3]. These network-based models revealed mechanistic insights and made novel predictions that were validated by follow-up experiments. Furthermore, we have developed novel theoretical concepts such as the concept of the stable motif, which forms the foundation of computational methods to determine the repertoire of long-time behaviors of biological systems and to identify nodes that can drive the system into a desired state [25-28].

Karanam et al. recently developed a graphical user interface to easily analyze Boolean models [29] and applied it to integrate a CO_2 signaling pathway into our previous ABA-induced closure model [3], as an approach to describe CO_2 signaling. While it is a good demonstration of their methodology, this preliminary model is not a rigorous representation of CO_2 signaling in that: (1) it lacks a comprehensive literature review to identify elements that are differentially regulated in high CO_2 signaling as compared to ABA signaling; (2) it assumes that high CO_2 is sufficient to directly activate water efflux through the membrane, as well as Ca^{2+} inflow, which together are sufficient to drive stomatal closure: these assumptions short-circuit all other CO_2-related nodes, i.e. render the rest of their network superfluous. Because of the assumed direct connection to water efflux, this model would fail to recapitulate, for example, the experimental observations of impaired high CO_2 induced closure for *ht1* [10] and *mpk4/12* [12] mutants. A more rigorous network construction approach is required to produce a more accurate representation and simulation of high CO_2 induced closure.

In this work, we compile and integrate an extensive body of literature evidence to assemble a guard cell signal transduction network that characterizes how high CO_2 induces stomatal closure. To further capture the dynamics involved in the stomatal closure process, we develop a dynamic model of the signaling network. We rigorously evaluate the accuracy of the model against known experimental observations, obtaining a high (91%) accuracy. We perform analyses including network connectivity, model simulation and stable motif analysis, which reveal a feedback core that dictates the cellular decisions in the CO_2 response, and the roles of key nodes in the process. We

bioRxiv preprint doi: https://doi.org/10.1101/2023.10.23.563079; this version posted October 25, 2023. The copyright holder for this preprint (which was not certified by peer review) is the author/funder, who has granted bioRxiv a license to display the preprint in perpetuity. It is made available under aCC-BY-NC 4.0 International license.

then demonstrate the predictive power of our network model by predicting the outcomes of numerous perturbations (e.g., node knockouts) that can potentially influence stomatal response; such predictions are valuable for the prioritization of wet bench experiments. Finally, we experimentally test and validate three predictions related to the role of NO in stomatal closure. A flowchart of our work is shown below (Figure 1). Our modeling framework captures system-level biological processes and provides insights into their logic and key underlying mechanisms.

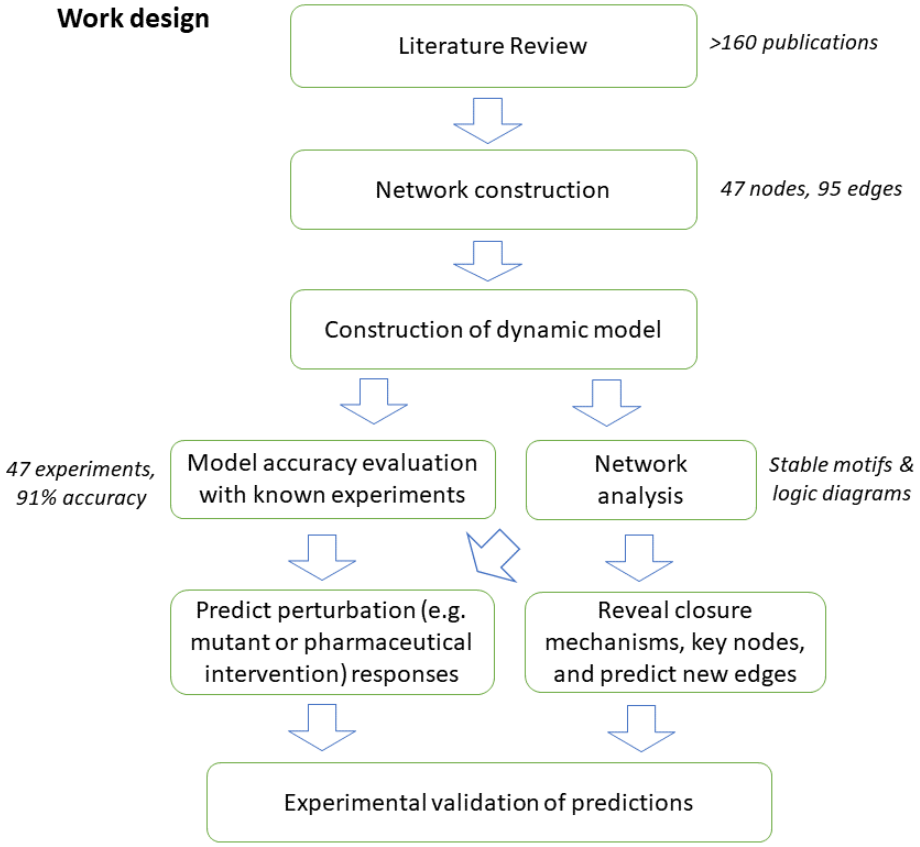

Figure 1 Flow chart of the overall work design. We construct a signaling network based on literature review, resulting in a network of 47 nodes and 95 edges. We then construct a Boolean dynamic model, which adds node states and regulatory logic to the network. We assess the accuracy of our network model by comparing its results with known experimental observations, finding that the model simulations successfully recapitulate 91% of experimental observations. We also perform multiple network-based analyses on the model. Finally, we experimentally validate selected model predictions.

II. Results

Construction and analysis of the signaling network of high CO_2-induced stomatal closure

We conducted a comprehensive literature review, covering more than 160 publications relating to stomatal closure or to elements of guard cell CO_2 signaling, and manually

bioRxiv preprint doi: https://doi.org/10.1101/2023.10.23.563079; this version posted October 25, 2023. The copyright holder for this preprint (which was not certified by peer review) is the author/funder, who has granted bioRxiv a license to display the preprint in perpetuity. It is made available under aCC-BY-NC 4.0 International license.

curated the interaction information from these publications (Supporting Info S1). Manual curation was necessary and important because not all guard cell signaling elements are equally relevant to high CO_2 induced closure. For example, cytosolic pH increases in response to ABA, but does not increase under high CO_2 [8, 30, 31]. Another example is the kinase OST1 (*Open Stomata1*/SnRK2.6), known to phosphorylate SLAC1 as a key contributor to the ion flow that leads to stomatal closure induced by ABA. Although *ost1* mutants show strongly impaired stomatal closure under both ABA and high CO_2, a recent study showed that unlike ABA, high CO_2 does not increase OST1 kinase activity in guard cells [32, 33].

To focus on CO_2 signaling, we divide the evidence into five categories based on relevance: (1) elements and their interactions that are validated to be involved in CO_2 signaling; (2) generic interactions that can be assumed to be involved in CO_2 signaling, e.g. chemical reactions whose reactants are reasonably expected to be present in the guard cell; (3) evidence that shows an element is not involved in CO_2 signaling; (4) evidence that supports an element's role in stomatal closure in response to another signal, but the element's involvement in high CO_2-induced closure has not been investigated; (5) evidence that supports an element's role in high CO_2 induced closure but this element has no or insufficient connections to elements in categories (1) and (2). The resulting list of observations and their categorization is provided in Supporting Info S1. We use category (1) and (2) evidence to construct the high CO_2 signaling network and exclude category (3) and (4) evidence. Category (5) evidence is also necessarily excluded, as it is not possible to connect such nodes to the network. Such categorization is also helpful to wet bench investigators; e.g., category 4 and 5 elements would be of particular interest to investigate further in the future.

To represent signaling elements with different functions, we deploy a multi-node representation for the OST1, MPK and SLAC1 proteins, separating the different (e.g., CO_2 -dependent and independent) mechanisms for their activation (see Figure *2*C for an example, and see Supporting Info S2 and S3 for details). As the follow-up analyses require that each edge of the network points to a node, during network construction we redirected each evidence of influence on an edge to an equivalent influence on the target of the edge [34].

bioRxiv preprint doi: https://doi.org/10.1101/2023.10.23.563079; this version posted October 25, 2023. The copyright holder for this preprint (which was not certified by peer review) is the author/funder, who has granted bioRxiv a license to display the preprint in perpetuity. It is made available under aCC-BY-NC 4.0 International license.

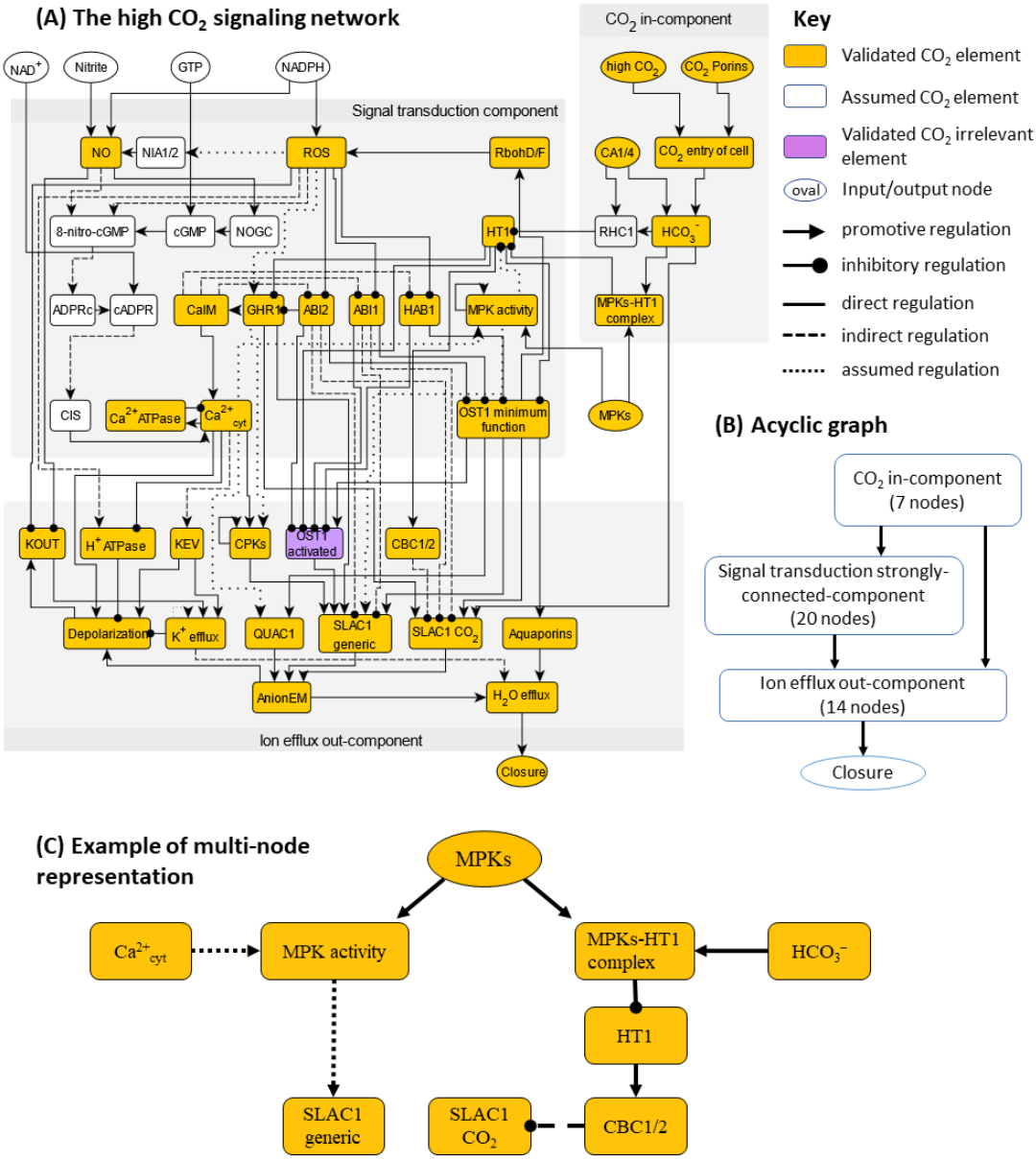

Figure 2. (A) The high CO_2 signaling network with 47 nodes and 95 edges. (B) Acyclic graph representation of the network highlighting the in-component, the strongly-connected-component and the out-component, forming a hierarchical structure of signal transduction; (C) Illustration of the multi-node representation of signaling elements that participate in multiple pathways and mechanisms, using MPKs as an example. MPKs are known to inhibit HT1 by a physical interaction induced by bicarbonate and independent of the MPKs' kinase activity [13, 14], and also are necessary in Ca^{2+}-induced SLAC1 activation [35].

Biological description of the high CO_2-induced stomatal closure network and its overlap with the ABA-induced closure network

The signaling network corresponding to high CO_2 induced closure contains 47 nodes and 95 edges (Figure 2A). A summary table of all edges is presented in Table 1. The full list of nodes and edges, including the full node names, is provided in Supporting

bioRxiv preprint doi: https://doi.org/10.1101/2023.10.23.563079; this version posted October 25, 2023. The copyright holder for this preprint (which was not certified by peer review) is the author/funder, who has granted bioRxiv a license to display the preprint in perpetuity. It is made available under aCC-BY-NC 4.0 International license.

Info S2. We mark nodes of the network (Figure 2A) in three colors, to reflect their specificity to high-CO_2 induced closure. Yellow nodes represent validated elements in CO_2 signaling, i.e., category (1); white nodes represent assumed elements based on generic evidence, i.e., category (2). Although by default nodes in categories (3) - (5) are not included in the network, "OST1 activated" is a member of a node pair (it represents increased kinase activity of OST1), thus we include it and mark it in purple to indicate that it belongs to category (4): it is not involved in high CO_2-induced closure but is important under ABA-induced closure.

The edges in the network are also marked to distinguish their properties: solid edges indicate a direct interaction/regulation, dashed edges indicate indirect regulation, and dotted lines indicate assumed regulation. An example of indirect regulation is the edge from ROS to the H^+ ATPase, which is dashed. An example of an edge referring to assumed regulation is the edge from HCO_3^- to SLAC1 CO_2, which is supported by a specific SLAC1 residue that is required for full CO_2 signaling and is structurally predicted to interact with HCO_3^- [36], but this predicted physical interaction has not been experimentally verified. Like this example, all assumed edges in the model are well-supported. Further justification of the assumed edges can be found in Supporting Info S3.

The high CO_2-induced stomatal closure network is known to share nodes and pathways with the ABA-induced closure network, but it also has its unique signaling elements. Furthermore, through the literature review process, we also found multiple elements that participate in ABA-induced closure but are not yet evaluated in the context of high CO_2 induced closure (also see Supporting Info S1 and S4). We list in Table *1* the different categories for the combined set of the signaling elements (i.e. nodes) of this CO_2 network and of our 2017 ABA network [3].

Table 1. Signaling elements that differ in the networks that lead to closure in response to ABA versus high CO_2.

Category	Nodes/signaling elements
CO_2-specific signaling elements that are not involved in ABA-induced closure	CA1/4, HCO_3^-, RHC1, HT1, MPKs-HT1 inhibition
ABA signaling elements observed to be absent or not significant in high CO_2-induced closure	Cytosolic pH increase, OST1 activation
ABA signaling elements* whose participation in high CO_2 signaling has not been tested	AtRAC1, actin reorganization, GPA1, Malate, Microtubule depolymerization, PEPC, PP2CA, ROP11, S1P/PhytoS1P, SPHK1/2, SLAH3, TCTP; *Phospholipases and molecules involved in reactions catalyzed by them:* PtdIns(4,5)P2, PLC, DAG, InsP3, InsP6, PLDα, PLDδ, PA; *Elements of the pathway leading to vacuolar acidification:* PI3P5K, PtdIns(3,5)P2, V-PPase, V-ATPase, vacuolar acidification;

bioRxiv preprint doi: https://doi.org/10.1101/2023.10.23.563079; this version posted October 25, 2023. The copyright holder for this preprint (which was not certified by peer review) is the author/funder, who has granted bioRxiv a license to display the preprint in perpetuity. It is made available under aCC-BY-NC 4.0 International license.

CO_2 signaling elements with insufficient regulatory information to integrate into our CO_2 network**	TPK1, KIN7, BIG1, AtABCB14, GCA2

*The full names of the ABA signaling elements can be found in [3].

** Details and references for these elements are provided in Supporting Info S1.

The CO_2 signaling network consists of three distinct modules

Of the 47 nodes in the network, 8 (including high CO_2) are source nodes that are not regulated by any other node, and one node (Closure) is a sink node (output). The source nodes other than the signal "high CO_2" mainly represent molecules needed as substrates for reactions incorporated in the network: CO_2 porins, CA1/4, GTP, MPKs, NAD^+, NADPH, Nitrite. Structural and connectivity analysis shows that the CO_2 network is organized into three graph modules (called "connected components" in graph theoretical language), as shown in Figure 2B. First, 7 early CO_2 signaling nodes form an in-component, i.e., these nodes are not regulated by any nodes from other components in the network. This module mainly represents how CO_2 enters the guard cell and is converted to HCO_3^-. Second, a large strongly-connected-component (SCC) of 20 nodes forms the core of the signal transduction network. "Strongly connected" means that for any node pair A, B, there is at least one regulatory path from A to B and at least one path from B to A. The feedback loops underlying the strong connectivity allows complex dynamical behavior that ultimately dictates the homeostasis of the system. The four edges between the in-component and the SCC represent CO_2 sensing mechanisms, e.g. the inhibitory effect of HCO_3^- on HT1 via the formation of the MPKs-HT1 complex. Third, 13 nodes, mainly representing ion transport mechanisms and the ion and water fluxes they mediate, as well as the output node "Closure", form the out-component that ultimately implements stomatal closure. These nodes are mainly regulated by nodes of the SCC and do not regulate nodes in other connected components. These three modules determine a higher-level overall linear structure of signal propagation from the in-component (which includes the input CO_2 signal) to the feedback-rich SCC, and finally to the out-component and closure (Figure 2B). The HCO_3^- activation of SLAC1 described in [36] forms a unique edge that connects the CO_2 in-component directly to the out-component.

Construction of the dynamic model

A network of signaling elements reveals the interactions and regulatory relationships between them, yet this alone is not sufficient to capture the dynamic aspects of signal transduction. In the stomatal closure process the biological system represented by the network evolves from a state corresponding to open stomata (in the absence of a closure signal) to a state corresponding to closed stomata after sufficient time has elapsed in the presence of a closure signal. To capture the dynamic state transition of the CO_2 network, we perform dynamic modeling, where we describe each node of the network with a state variable that represents its abundance or activity. In this way, the propagation of the high CO_2 signal is captured in the model by a series of node state changes propagating through the network, eventually leading to stomatal closure. We

bioRxiv preprint doi: https://doi.org/10.1101/2023.10.23.563079; this version posted October 25, 2023. The copyright holder for this preprint (which was not certified by peer review) is the author/funder, who has granted bioRxiv a license to display the preprint in perpetuity. It is made available under aCC-BY-NC 4.0 International license.

use a Boolean model, i.e., we describe each node with binary states: ON or 1 for higher-than-threshold abundance or activity; OFF or 0 for lower-than-threshold abundance and activity. Despite its simplicity, Boolean dynamics has proved capable of capturing complex biological behaviors [37], e.g. cell differentiation as a consequence of multi-stability [38, 39], or sustained oscillations such as the cell cycle [40].

For each node, its state change is determined by the regulatory influences incident on it, which are captured by its Boolean regulatory function. The regulatory function uses the states of the node's regulators in the network as inputs and combines these inputs using logical operators such that the function correctly reflects experimental observations. For example, the node "HCO_3^-" represents bicarbonate concentration in the guard cell. Its input nodes are "CO_2 entry of cell" and "CA1/4" (the CO_2-binding carbonic anhydrase enzymes CA1 and CA4). Since bicarbonate is produced from the reaction $CO_2 + H_2O \rightarrow HCO_3^- + H^+$, catalyzed by CA1/4, we know that both CO_2 entry into the cell and CA1/4 are required for the increase of intracellular bicarbonate concentration, thus the inputs are connected with a logical "AND" operator, and the regulatory function of node "HCO_3^-" is set as "$f_{HCO_3^-}$ = CA1/4 AND CO2 entry of cell". The comprehensive list of regulatory functions and their justifications are provided in Supporting Info S3. Each node's regulatory function determines the future state of the node as determined by the current state of its regulators.

With the Boolean regulatory functions defined for each node, we can perform simulations of the signal transduction process over the entire CO_2 network. We initialize the *in silico* stomata in a pre-stimulus, i.e. open state, with an ON state for closure-inhibiting nodes (namely ABI1, ABI2, CBC1/2, HAB1, HT1, and H^+ ATPase) and other nodes OFF (see Supporting Info S3 for the complete initial condition). We deploy a discrete-time simulation, with stochastic random order asynchronous update, and simulate the network model for 30 timesteps (see Methods). Each simulated trajectory of the model will eventually converge into a stabilized behavior of the system as a whole, called an attractor. The most intuitive attractor is a steady state, where all nodes stabilize in a fixed state. Alternatively, a system can also have an oscillatory attractor, where a fraction of nodes indefinitely oscillate between 0 (OFF) and 1 (ON). A system can have multiple attractors (called multi-stability), which may be reachable from the same initial state if the system's timing is stochastic. We obtain the consensus behavior of the system by performing 1000 replicate simulations, i.e., 1000 "*in silico* stomata" simulations starting in the same pre-stimulus state, then calculating the percentage of node activation at each timestep as our metric, meaning the percentage of simulations in which the node (e.g. Closure) is in state 1 (ON). In this way, oscillations and multi-stability with different node states will display a percentage of node activation with a value between 0% and 100%. We demonstrate simulated high CO_2 induced stomatal closure and lack of closure under ambient CO_2 in Figure 3Figure *2*B, and show a summary of node states in the corresponding attractors in Figure 3C.

bioRxiv preprint doi: https://doi.org/10.1101/2023.10.23.563079; this version posted October 25, 2023. The copyright holder for this preprint (which was not certified by peer review) is the author/funder, who has granted bioRxiv a license to display the preprint in perpetuity. It is made available under aCC-BY-NC 4.0 International license.

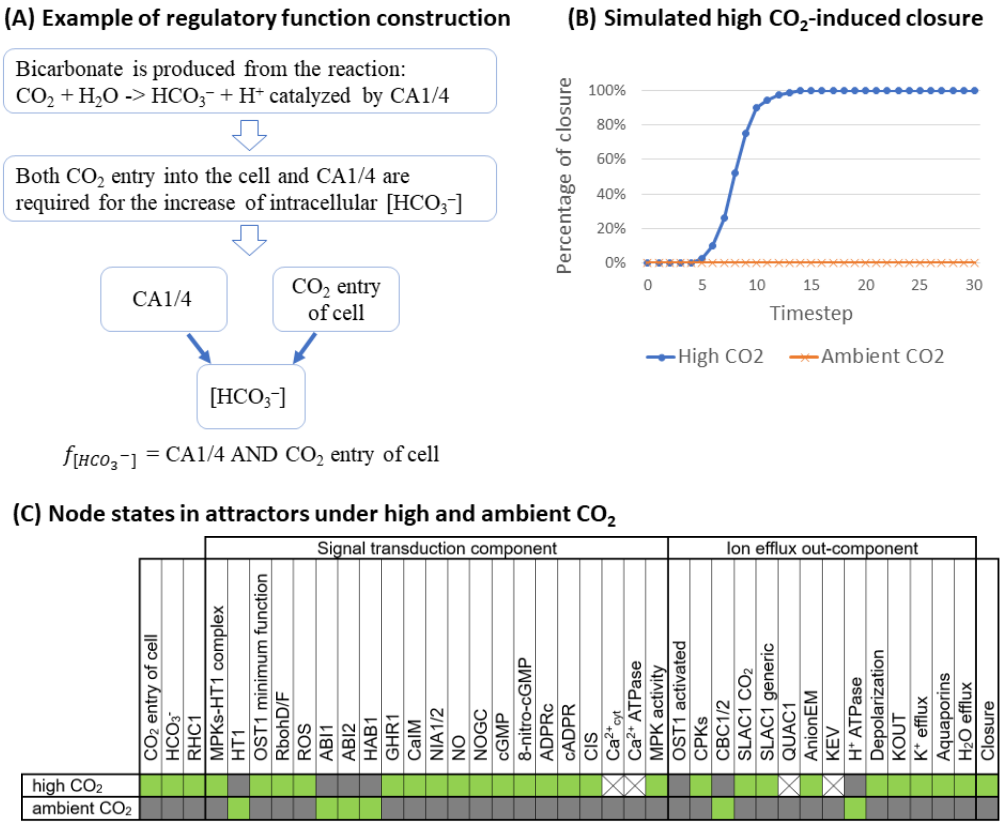

Figure 3 (A) Example demonstrating how a Boolean regulatory function is constructed from observations; (B) A demonstration of model simulation, capturing stomatal closure under high CO_2, and lack of closure under ambient CO_2; (C) Summary of node states in the attractor with closure ON under high CO_2, and the attractor with closure OFF under ambient CO_2, found from the model simulations. A green box represents the ON state, grey represents the OFF state, and X represents oscillation.

In the simulated wild-type system (Figure 3B), the percentage of closure in response to high CO_2 increases over the timesteps from 0% to 100%. Despite the deliberate choice of stochasticity in the timing, all the simulations converge into the same attractor, in which the node Closure is ON. The row marked "high CO_2" in Figure 3C shows the states of all nodes in this attractor, recapitulating the biological knowledge regarding the activity of nodes in stomata that closed in response to high CO_2. For example, the node "OST1 activated" is OFF in this closure attractor, meaning that OST1 does not become activated under high CO_2, consistent with recent publications [32, 33]. The node Ca^{2+}_{cyt} oscillates between ON and OFF, capturing transient cytosolic Ca^{2+} concentration increases that have been observed during CO_2 response [17, 18]. We observe that the node "SLAC1 generic" is activated (as all of its regulators, including CPKs, are indirectly activated by high CO_2). Conversely, in the simulation curve corresponding to ambient CO_2 (represented as the inactivity of the node "high CO_2") the percentage of closure remains 0% for the entire duration of the simulation, consistent with the expectation that stomata are open in the absence of CO_2

bioRxiv preprint doi: https://doi.org/10.1101/2023.10.23.563079; this version posted October 25, 2023. The copyright holder for this preprint (which was not certified by peer review) is the author/funder, who has granted bioRxiv a license to display the preprint in perpetuity. It is made available under aCC-BY-NC 4.0 International license.

elevation. The row marked "ambient CO_2" in Figure 3C shows the states of all nodes in the attractor under ambient CO_2.

Validation of the network model

We assembled all experimental evidence related to high CO_2 induced stomatal closure that was not used in model construction (see the entries with "V" for validation, in Supporting Info S1), and checked if the model simulations of the relevant settings yield results consistent with the experimental evidence. An important concept that can be insufficiently appreciated by experimentalists is that all the pathway-level effects (e.g., the effect of a node manipulation on high CO_2 induced stomatal closure) are emergent properties of the system that arise from multiple interactions; thus, the fact that the regulatory functions of each node are informed by experimental evidence is not sufficient to guarantee consistency with pathway-level observations.

The summary of validation and consistency is presented in Table 2. In a total of 47 settings, there are 43 cases of consistency between the experimental and simulation results and 4 inconsistent cases, yielding an accuracy of 43/47 = 91%. The high validation accuracy shows that our model correctly captures most known signaling behaviors in CO_2-induced stomatal closure. Note that a few comparisons could be consistent by construction if the observed regulator node directly regulates the target node in the model. When assessing the validity of our model, we exclude this type of trivial consistency. A more detailed validation table including the trivially consistent cases, a description of each experimental observation, and explanations are provided in Supporting Info S5.

Table 2 Comprehensive validation comparing simulations against known experimental observations. In the 47 total simulations in the table, 43 are consistent, 4 are inconsistent (marked with bold, underlined font), with accuracy 43/47 = 91% here.

Row #	Signal	Simulation setting	Experimental outcome	Ref	Simulated percentage of node
1.	High CO_2	MPKs = OFF	No closure	[12, 16]	Closure=0%
2.	High CO_2	MPK activity = OFF	Closure	[13, 14]	Closure=100%
3.	High CO_2	MPK activity = ON	Closure	[14]	Closure=100%
4.	High CO_2	MPK activity = OFF, MPKs-HT1complex = OFF	No or reduced closure	[14]	Closure=0%
5.	High CO_2	HT1 = OFF	Closure	[9, 11]	Closure=100%
6.	High CO_2	HT1 = ON	No closure	[10, 11]	Closure=0%
7.	High CO_2	RHC1=OFF, HT1=OFF	SLAC1 CO_2 activation	[15]	SLAC1 CO_2=100%
8.	High CO_2	HT1=OFF, OST1 minimum function=OFF	No or reduced Closure	[15]	Closure=0%
9.	High CO_2	CBC1/2 OFF	Closure	[13]	Closure=100%
10.	High CO_2	CBC1/2 OFF, HT1 = ON	Closure	[13]	**Closure=0%**
11.	High CO_2	CA14 = OFF	Reduced closure	[7]	Closure=0%
12.	High CO_2	CA14 = OFF, HT1=OFF	Closure	[7]	Closure=100%
13.	High CO_2	GHR1 = OFF	Reduced closure	[11, 41]	Closure=41.5%
14.	High CO_2	HCO_3^-=OFF, high CO_2 = ON	SLAC1 OFF	[8]	SLAC1 generic=0%, SLAC1 CO_2=0%
15.	High CO_2	Ca^{2+}_{cyt} = OFF	No closure	[17-19]	Closure=0%
16.	High CO_2	ABI1 = ON	Reduced closure	[42, 43]	Closure=44.0%

bioRxiv preprint doi: https://doi.org/10.1101/2023.10.23.563079; this version posted October 25, 2023. The copyright holder for this preprint (which was not certified by peer review) is the author/funder, who has granted bioRxiv a license to display the preprint in perpetuity. It is made available under aCC-BY-NC 4.0 International license.

Row #	Signal	Simulation setting	Experimental outcome	Ref	Simulated percentage of node
17.	High CO_2	ABI2 = ON	No closure	[42, 43]	Closure=39.9%
18.	High CO_2	Default (high CO_2 =ON)	$Ca^{2+}_{cyt} > 0$	[17]	Ca^{2+}_{cyt} = 53.6% (oscillating)
19.	High CO_2	ROS=OFF	Reduced closure	[20]	Closure=0%
20.	High CO_2	RbohD/F = OFF	Reduced closure	[20, 44]	Closure=0%
21.	High CO_2	OST1 minimum function= OFF	No closure	[8]	Closure=0%
22.	High CO_2	Aquaporins = OFF	No closure	[6]	Closure=0%
23.	High CO_2	CO_2 porins = OFF	No closure	[6]	Closure=0%
24.	High CO_2	Default (high CO_2 =ON)	Anion efflux ON	[30]	AnionEM=100%
25.	High CO_2	Default (high CO_2 =ON)	K^+ efflux is ON	[30]	K^+ efflux=100%
26.	High CO_2	QUAC1 = OFF	Slower closure	[45]	Closure reaches 100% more slowly than WT
27.	High CO_2	CPKs = OFF (CPK 4,6,21,23)	Closure	[46]	Closure=100%
28.	High CO_2	Default (high CO_2 =ON)	ROS is produced	[20, 21]	ROS= 100%
29.	High CO_2	GHR1 = OFF, HT1 = OFF	No or reduced Closure	[11]	Closure=43.9%
30.	High CO_2	NO=OFF	Reduced closure	[22]	**Closure=100%**
31.	High CO_2	SLAC1 CO_2=OFF, SLAC1 generic=OFF	No closure	[47, 48]	Closure=43.9%
32.	High CO_2	SLAC1 CO_2=OFF, SLAC1 generic=OFF, QUAC1=OFF	No closure	[48]	Closure=0%
33.	High CO_2	R256 residue mutation interpreted as SLAC1 CO_2=OFF	Reduced closure	[36]	**Closure reaches 100% more slowly than WT**
34.	High CO_2	Default (high CO_2 =ON)	H^+-ATPase deactivation	[49]	H^+-ATPase=0%
35.	Ca^{2+}	MPKs KO, high CO_2 = OFF, CaIM = ON	Reduced AnionEM	[35]	AnionEM=49.2%
36.	Ca^{2+}	RHC1 = OFF, CaIM = ON, high CO_2= OFF	Closure	[15]	Closure=100%
37.	Ca^{2+}	GHR1 = OFF, CaIM = ON, high CO_2= OFF	Closure	[50]	**Closure=40.3%**
38.	Ca^{2+}	CaIM = ON, high CO_2=OFF	Closure	[19]	Closure=100%
39.	Ca^{2+}	CPKs = OFF, CaIM =ON, high CO_2 = OFF	Reduced closure	[19]	Closure=41.1%
40.	ROS	GHR1 = OFF, ROS = ON, high CO_2 = OFF	No closure	[50]	Closure=41.2%
41.	ROS	ROS=ON, high CO_2=OFF	Closure	[44, 51]	Closure=100%
42.	ROS	ROS=ON, RbohD/F=OFF	Closure	[44]	Closure=100%
43.	NO	NO=ON, high CO_2=OFF	Closure	[51, 52]	Closure=100%
44.	8-nitro-cGMP	8-nitro-cGMP = ON, high CO_2=OFF	Closure	[53]	Closure=100%
45.	cADPR	cADPR = ON, high CO_2=OFF	Closure	[54]	Closure=100%
46.	HCO_3	HCO_3^-=ON, high CO_2 = OFF	SLAC1 activation	[7]	SLAC1 CO_2=100%
47.	HCO_3	MPKs=OFF, high CO_2=OFF, HCO_3^-=ON	Impaired SLAC1	[11, 12, 16]	SLAC1 generic=0%, SLAC1 CO_2=0%

Network-based analysis identifies the dynamic repertoire and decision-making mechanisms of the CO_2 signaling system

In the previous section we showed that our model can accurately reproduce existing experimental observations. Next, we explore the explanatory power of the model and its predictions about the biological system's response in conditions for which experimental observations are not yet available.

We start by determining the full attractor repertoire of the model. The attractor repertoire of the model is important because attractors correspond to biological phenotypes, e.g., open or closed stomata are represented by two different attractors in the CO_2 network model. Finding the attractor repertoire is the first step toward understanding how a biological system makes decisions on how to switch between

bioRxiv preprint doi: https://doi.org/10.1101/2023.10.23.563079; this version posted October 25, 2023. The copyright holder for this preprint (which was not certified by peer review) is the author/funder, who has granted bioRxiv a license to display the preprint in perpetuity. It is made available under aCC-BY-NC 4.0 International license.

different phenotypes. Understanding the decision-making behind attractor transitions of a biological system can reveal the key signal transduction mechanisms and suggest potential interventions to guide the system into a more desirable state. Finding attractors by simulations is difficult because the state space of a network model increases exponentially with its size, e.g., the CO_2 network model with 48 nodes has a total of 2^{48} states. An alternative and efficient way to find the attractors of a system is to utilize the network topology via stable motif analysis, developed by the Albert group [55]. Stable motifs are special feedback loops in a dynamic model that can self-sustain once their constituent nodes attain an associated state (see Methods). The important feature of stable motifs is that they are irreversible: after locking in they become independent of the rest of the system. This feature implies that the lock-in of a stable motif is like a decision of the system, and a series of stable motif lock-ins will lead to an attractor [26, 28, 55]. Therefore, finding all stable motifs and their lock-in sequence allows comprehensive identification of attractors.

Stable motifs identify the dynamic repertoire and decision-making of the system

Whether in ambient or high CO_2, the unperturbed (wild type) system has a stable motif (see Figure 4A) that includes the activity of RbohD/F and ROS, the minimum functional level of OST1, and the inactivity of the three PP2C protein phosphatases (ABI1, ABI2 and HAB1). We will refer to this stable motif as the Main Stable Motif (MSM). The lock-in of the MSM is observed in the closure ON attractor (the first row of Figure *3*C). The opposite states of the nodes involved in the MSM, namely the inactivity of RbohD/F, ROS, CaIM, and GHR1, the lack of OST1 function, and the activation of one of the PP2C protein phosphatases, form three instances of a weaker type of stable motif, called a conditionally stable motif [56] (see Methods). Figure 4B indicates the superposition of the three conditionally stable motifs and shows that they can lock-in if HT1 is ON. The lock-in of these conditionally stable motifs leads to the attractor with closure OFF (second row in Fig. 3C), which is consistent with the CO_2-independent high stomatal conductance of the *ht1-3D* and *ht1-8D* dominant mutants [10, 11]. Importantly, the MSM and the three conditionally stable motifs are mutually exclusive. Since the lock-in of a stable motif is irreversible, the choice between them constitutes the decision-making process of the CO_2 signaling network (Figure 4C). The system has additional (conditionally) stable motifs that contribute in specific circumstances; these are described in section II of Supporting Info S4.

bioRxiv preprint doi: https://doi.org/10.1101/2023.10.23.563079; this version posted October 25, 2023. The copyright holder for this preprint (which was not certified by peer review) is the author/funder, who has granted bioRxiv a license to display the preprint in perpetuity. It is made available under aCC-BY-NC 4.0 International license.

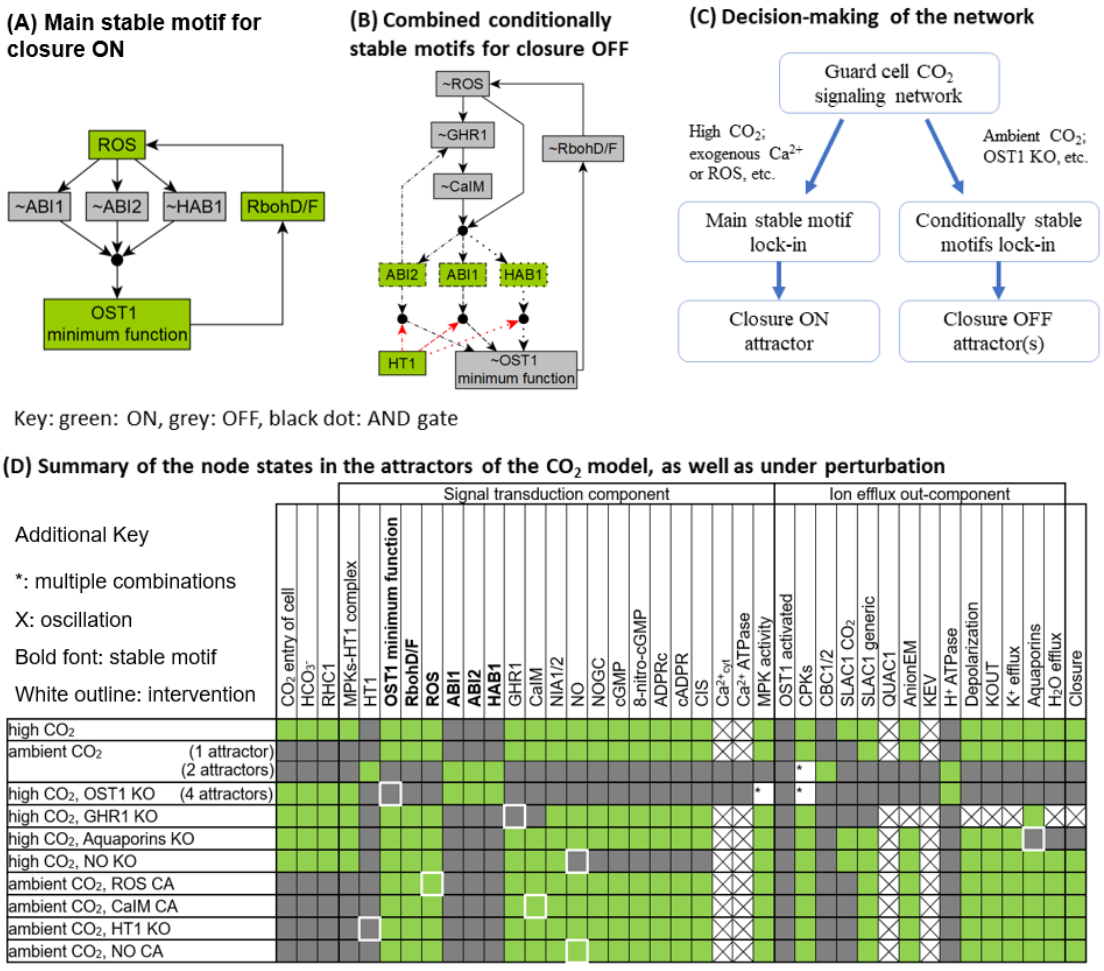

Figure 4. Stable motifs of the network model. (A) The main stable motif that leads to closure in the dynamic model. (B) Superposition of the three overlapping conditionally stable motifs that lead to attractors that represent open *in silico* stomata. Each conditionally stable motif contains a different PP2C protein family member, indicated by dashed, dash-dotted or dotted outline and edges, respectively. In the stable motifs, nodes whose name is preceded by ~ are inactive in the corresponding motif. The black circles indicate that the regulatory effects incident on a node form an AND gate; for example, ABI1 will activate only if ROS and CaIM are simultaneously inactive. The red edges starting from HT1 indicate that HT1=ON is the condition necessary for the conditionally stable motifs. (C) Decision-making diagram of the CO_2 signaling network. (D) Summary of the node states in the attractors of the system. Entries that contain a white box with * summarize multiple attractors in which the marked nodes take either on or off states.

Identifying the stable motifs allows comprehensive identification of all attractors of the system, using the algorithm developed in [27]. We first confirm the unique Closure ON attractor in the presence of high CO_2 (Figure *4*D), where high CO_2 leads to the locking-in of the Main Stable Motif and precludes the activation of the three conditionally stable motifs. The MSM leads to the activation of anion flow through the SLAC1 channel and to K^+ efflux, as well as to the activation of Aquaporins, which

bioRxiv preprint doi: https://doi.org/10.1101/2023.10.23.563079; this version posted October 25, 2023. The copyright holder for this preprint (which was not certified by peer review) is the author/funder, who has granted bioRxiv a license to display the preprint in perpetuity. It is made available under aCC-BY-NC 4.0 International license.

together satisfy all requirements to activate the node Closure. In the case of ambient CO_2, stable motif analysis identifies 3 attractors. Two of them have the node Closure OFF, corresponding to the absence of stomatal closure observed under ambient CO_2. These two attractors differ only in the state of CPKs (either ON or OFF). Interestingly, the 3rd attractor under ambient CO_2 has the node Closure ON, and is highly similar to the closure ON attractor under high CO_2 -- they differ only in the CO_2 in-component (see Figure *4*D, row 2 vs. row 1). Trajectories starting from the pre-stimulus initial state used in our simulation cannot reach this attractor under ambient CO_2, consistent with biological reality and with the attractor found by simulation (Figure 3C). Yet, a different initial state can lead to this attractor (see Supporting Info S3). An intervention (e.g., sustained activation of a node) can also induce stomatal closure under ambient CO_2, as we will present later.

Logic diagrams elucidate signal transduction mechanisms and the roles of driver nodes

To better understand how the system reaches its attractors (e.g., the closure ON attractor under ambient CO_2), we introduce logic diagrams illustrating the signaling mechanisms (Figure 5). A logic diagram (see Methods) is an integration of the network and node states that yield a specific outcome (e.g., the ON state of the node Closure), constructed based on the framework of the "expanded network" developed by the Albert group [55, 57, 58]. Edges in the logic diagrams are logical implications (i.e., sufficient activations), and black dots represent AND gates. To make the logic diagrams easier to parse, we also applied network reduction techniques that do not change the dynamic behavior of the system [59], and we merged nodes that behave similarly or as a group (e.g. PP2Cs, see Methods).

As shown in Figure 5A, high CO_2 activates the MSM (shown with bold font), which leads to ion and water efflux, and thus to an attractor with the node Closure ON. Figure 5B shows the mechanism for the lack of stomatal closure, e.g., under ambient CO_2. When HT1 is ON, the conditionally stable motifs (bold-font nodes, with their dependence on HT1=ON shown with red dotted edges) can lock in and cause the inactivity of the SLAC1 and QUAC1 channels, thus reaching a Closure OFF attractor. The knockout of OST1 also activates the conditionally stable motifs and leads to a similar Closure OFF attractor (see the third entry of Figure *4*D). In addition to attractors with constant closure values (constant ON or OFF), the system also allows attractors with an unstable closure value that oscillates between ON and OFF indefinitely. Figure 5C shows the logic diagram of the predicted mechanism of unstable Closure state that could arise from the sustained inactivity of the SLAC1 channels (due, e.g., to knockout of GHR1, see the fourth entry of Figure *4*D). The oscillation of Ca^{2+}_{cyt} leads to oscillating QUAC1 and K^+ efflux, which in turn lead to an oscillating Closure state. Had SLAC1 been active, it would have sustained anion efflux, leading to sustained Closure ON.

bioRxiv preprint doi: https://doi.org/10.1101/2023.10.23.563079; this version posted October 25, 2023. The copyright holder for this preprint (which was not certified by peer review) is the author/funder, who has granted bioRxiv a license to display the preprint in perpetuity. It is made available under aCC-BY-NC 4.0 International license.

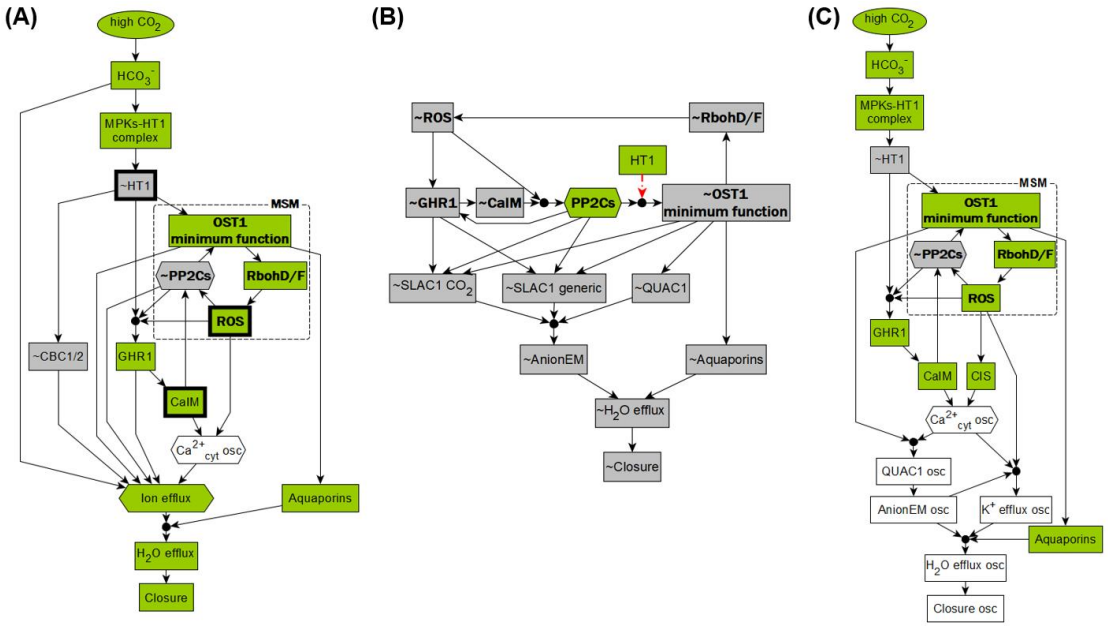

Figure 5. The logic diagrams show the mechanisms that lead to various stomatal behaviors. (A) Logic diagram of high CO_2-induced stomatal closure. It also indicates that a closure attractor can be reached under ambient CO_2 if the Main Stable Motif is activated by an internal or external driver. Three such drivers (out of 17) are indicated by bold outlines. (B) Diagram of the mechanism for the lack of closure due to the activation of the conditionally stable motifs, e.g., under ambient CO_2 or for *ost1* KO. (C) Logic diagram of the predicted mechanism of unstable closure that would arise with inactivity of the SLAC1 channels. Green nodes indicate the active state and grey means the inactive state; white nodes oscillate.

In addition to finding attractors, stable motif analysis can also pinpoint key nodes called drivers, which determine the decisions in the system: once a driver node is sustained in a certain state, it can lock in a corresponding stable motif, forcing a decision in the system. Thus, external control of driver nodes can drive the system from one attractor to another [25, 27]. For example, ROS (marked in bold outline) is an internal driver of the MSM, as it inhibits all three PP2C proteins, which then allows OST1 activity, which in turn activates RbohD/F, closing the cycle of self-sustained activity. Furthermore, CaIM (Ca^{2+} influx through the membrane) is an external driver of the MSM, as it inhibits the PP2Cs. When ROS or Ca^{2+} is externally provided, it will lock in the MSM, thus lead to a closure ON attractor, even in ambient CO_2 (see Figure *4*D). This explains the experimentally observed ROS or Ca^{2+} induced stomatal closure under ambient CO_2 [19, 44, 60]. Moreover, ~HT1 (the OFF state of HT1) is also an external driver of the MSM, and leads to the same closure ON attractor as providing ROS or Ca^{2+} (see Figure *4*D), which explains the low stomatal conductance observed in the *ht1-2* kinase dead mutant regardless of the CO_2 concentration [9].

Our model predicts how the perturbation of signaling elements affects high CO_2 response

bioRxiv preprint doi: https://doi.org/10.1101/2023.10.23.563079; this version posted October 25, 2023. The copyright holder for this preprint (which was not certified by peer review) is the author/funder, who has granted bioRxiv a license to display the preprint in perpetuity. It is made available under aCC-BY-NC 4.0 International license.

A model is most helpful in predicting unknown behaviors of a system. We first demonstrate the predictive power of our model by simulating the guard cell response to high CO_2 under systematic single node perturbations. These simulations reflect how mutations or interventions could affect high CO_2 induced closure. We simulate all single interventions that abolish a node's expression or activity as maintaining the node in the state 0 (OFF) and denote it "KO"; we also simulate all single interventions that make a node constitutively active by maintaining the node in the state 1 (ON) and denote it "CA". To quantify the stomatal closure response, we develop an improved approach from [3] combining three metrics: the final closure state, the cumulative percentage of closure (CPC), as well as the attractor repertoire of the system (see Methods). The CPC value represents the fraction of simulations in which Closure = 1, summed over 30 timesteps, thus it ranges from 0 to 30. As before [3, 61], we observe and categorize four typical behaviors different than the wild type (WT) response: (1) we call the behavior in which the percentage of closure increases faster than in the WT system "hypersensitivity", and (2) the behavior in which the percentage of closure increases more slowly than in the WT system "hyposensitivity"; (3) we refer to the behavior in which the percentage of closure converges to or oscillates around an intermediate value "reduced closure"; (4) and finally the category "no closure" is the lack of closure in simulated stomata. We present the summarized high CO_2 closure response categories under systematic perturbations in Figure 6A. The complete perturbation results can be found in Supporting Info S6. We illustrate simulated response curves of these categories in Figure 6B: hypersensitivity under external Ca^{2+} (CaIM CA), hyposensitivity under CaIM KO, reduced closure under H^+-ATPase KO, and no closure under MPKs KO (*mpk4/12* mutant). These perturbation response categories offer a way to characterize each signaling element's contribution to high CO_2 induced closure, from weakest (nodes whose KO and CA are in the "Close to WT" category, such as cGMP) to strongest (nodes whose KO is in the "No closure" category and whose CA is in the "Hypersensitivity" category, such as ROS).

bioRxiv preprint doi: https://doi.org/10.1101/2023.10.23.563079; this version posted October 25, 2023. The copyright holder for this preprint (which was not certified by peer review) is the author/funder, who has granted bioRxiv a license to display the preprint in perpetuity. It is made available under aCC-BY-NC 4.0 International license.

(A)

Response	Node perturbation
Close to WT CPC range: 20.405 to 20.709 Final closure = 1	8-nitro-cGMP KO, ABI1 KO, ABI2 KO, ADPRc KO, Aquaporins CA, CA1/4 CA, cADPR KO, CBC1/2 KO, cGMP KO, cGMP CA, CIS KO, CO_2 porins CA, CPKs KO, CPKs CA, GTP KO, GTP CA, HAB1 CA, H^+ATPase KO, HAB1 KO, MPKs CA, MPK activity KO, NAD^+ KO, NAD^+ CA, NADPH CA, NIA1/2 KO, Nitrite KO, Nitrite CA, NO KO, NOGC KO, NOGC CA, OST1 activated KO, OST1 activated CA, RHC1 KO, SLAC1 $nonCO_2$ KO
Hypersensitivity CPC>20.709 Final closure = 1	8-nitro-cGMP CA, ADPRc CA, AnionEM CA, Ca^{2+}ATPase KO, Ca^{2+}_{cyt} CA, cADPR CA, CaIM CA, CIS CA, CO_2 entry of cell CA, Depolarization CA, GHR1 CA, H_2O Efflux CA, HCO_3^- CA, HT1 KO, K^+efflux CA, KEV CA, KOUT CA, MPKs-HT1complex CA, MPK activity CA, NIA1/2 KO, NIA1/2 CA, NO KO, NO CA, OST1 minimum function CA, QUAC1 CA, RbohD/F CA, RHC1 CA, ROS CA, SLAC1 CO_2 CA, SLAC1 $nonCO_2$ CA
Hyposensitivity CPC range: 18.379-20.405 Final closure = 1	CaIM KO, CBC1/2 CA, QUAC1 KO, SLAC1 CO_2 KO
Reduced closure CPC range: 7.126- 8.580 Final closure between (0,1)	ABI1 CA, ABI2 CA, GHR1 KO, H^+ATPase CA
No closure CPC = 0 Final closure = 0	AnionEM KO, Aquaporins KO, Ca^{2+}ATPase CA, CA1/4 KO, Ca^{2+}_{cyt} KO, CO_2 porins KO, CO_2 entry of cell KO, Depolarization KO, HT1 CA, H_2O Efflux KO, HCO_3^- KO, K^+efflux KO, KEV KO, KOUT KO, MPKs-HT1complex KO, MPKs KO, NADPH KO, OST1 minimum function KO, RbohD/F KO, ROS KO

(B) Simulated examples of closure response to high CO_2 and under perturbation

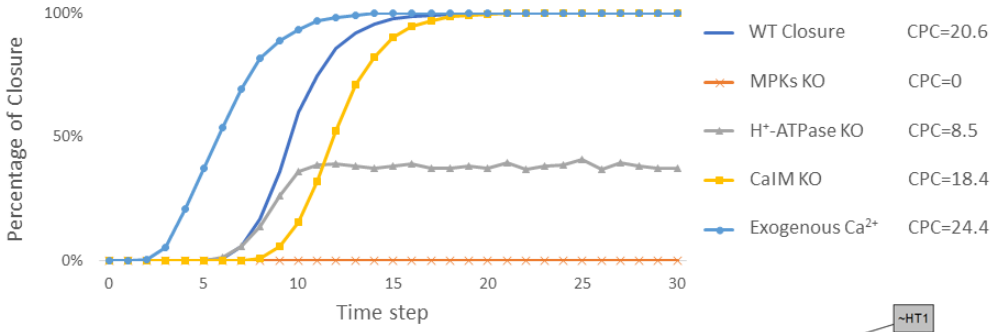

(C) Predicted perturbations that can induce closure under ambient CO_2

8-nitro-cGMP CA, ADPRc CA, Ca^{2+}_{cyt} CA, **cADPR CA**, **CaIM CA**, CIS CA, CO_2 entry of cell CA, GHR1 CA, H_2O Efflux CA, **HCO_3^- CA**, **HT1 KO**, MPKs-HT1complex CA, MPK activity CA, NIA1/2 CA, **NO CA**, OST1 minimum function CA, RbohD/F CA, **ROS CA**

Bold: supported by evidence in the literature
Bold and underlined: validated in a study dedicated to high CO_2 signaling

(D)

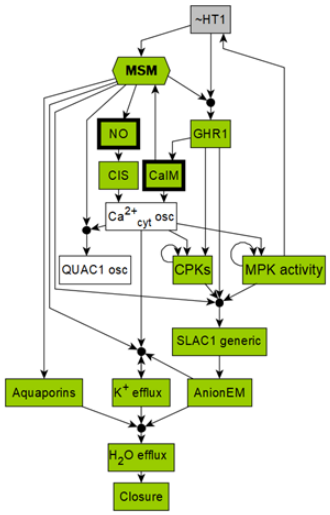

Figure 6. Systematic perturbation under high CO_2 with illustrations. (A) Response categorization for systematic perturbations of all nodes (both KO and CA perturbations). (B) Simulation curves under high CO_2 that exemplify response types: normal WT closure, hypersensitivity under external Ca^{2+} (Ca^{2+} influx across the membrane (CaIM) CA), hyposensitivity under CaIM KO, reduced CO_2 sensitivity for H^+-ATPase, or insensitivity to CO_2 under MPKs KO. (C) Model simulation predicts 18 interventions that could induce stomatal closure under ambient CO_2. Bolded interventions have supporting evidence in previous publications, and bolded plus underlined interventions have been validated to induce closure under ambient CO_2.

bioRxiv preprint doi: https://doi.org/10.1101/2023.10.23.563079; this version posted October 25, 2023. The copyright holder for this preprint (which was not certified by peer review) is the author/funder, who has granted bioRxiv a license to display the preprint in perpetuity. It is made available under aCC-BY-NC 4.0 International license.

(D) Logic diagram of the mechanism of closure in ambient CO_2. The node "MSM" is a merged representation of the Main Stable Motif. Bold outlines indicate 2 of the 18 interventions that can simultaneously activate the MSM and inactivate HT1 under ambient CO_2. For example, NO leads to oscillations in Ca^{2+}_{cyt}, which lead to MPK activity, which inactivates HT1, which then activates the MSM and leads to closure.

The five response categories are well-explained by our stable motif and network analysis

We find that in both hyper- and hypo-sensitivity cases, the final attractor of the system is almost the same as that of the wildtype system under high CO_2; the final attractor only differs in the state of the perturbed node and up to a few other nodes regulated by it. As illustrated in the logic diagrams (Figure 5) earlier, the typical reason for hyper-sensitivity (i.e., faster closure) is the immediate accomplishment of a node state that would naturally happen only after a previous event; e.g., CaIM normally would only happen after GHR1 activation (Figure 5A), but it happens immediately with CaIM CA. The mechanism for slower closure is the elimination of one of two redundant signaling pathways: for example, CaIM KO will eliminate one pathway to increase the cytosolic Ca^{2+} level (a necessary condition of closure); the alternative pathway to activate Ca^{2+}_{cyt} is by CIS (Ca^{2+} influx from stores). The model prediction that perturbation of specific anion channels, e.g. QUAC1 KO or R256 residue KO (interpreted as SLAC1 CO_2=OFF) leads to hyposensitivity is due to the same type of mechanism. Reduced closure occurs when the state of the node Closure oscillates in all attractors, such as for GHR1 KO (see row 6 in Figure *4*D and Figure 5C). GHR1 KO leads to the deactivation of the SLAC1 anion channel, leaving QUAC1 as the only conduit of anion flow, and the activity of QUAC1 follows the Ca^{2+}_{cyt} oscillation, resulting in an attractor with oscillatory closure. The final category of behavior, "no closure", is the lack of closure in all simulated stomata; the system converges into an attractor (or mix of attractors) with closure OFF. The mechanism that leads to this outcome is disruption of ion or water efflux, either through a mutation in a transporter (e.g., Aquaporins KO in Figure *4*D), or indirectly through activation of the non-closure conditionally stable motifs (e.g., OST1 KO in Figure *4*D; the mechanism is illustrated in Figure 5B).

Our model predicts interventions that yield closure even under ambient CO_2

We performed systematic perturbation simulations of the model under ambient CO_2 (i.e. with the node "high CO_2" set to OFF), and found 18 interventions that can result in Closure=ON in the simulations (Figure *6*C; comprehensive results are in Supporting Info S6). Our stable motif analysis identifies that the reason for the effectiveness of these interventions is the activation of the MSM coupled with the inactivation of HT1 (see Figure 5A). HT1 KO itself is an example of such a stable-motif-activating intervention; this result agrees with the closed stomata or low stomatal conductance observed in the *ht1-2* mutant [9, 11]. Thus, the model predicts that constitutive activity of the nodes that lead (directly or indirectly) to the inhibition of HT1 can also drive the stable motifs and lead the system to closure in ambient CO_2. Indeed, all the interventions listed in Figure 6C have this property. Figure *4*D illustrates the Closure

bioRxiv preprint doi: https://doi.org/10.1101/2023.10.23.563079; this version posted October 25, 2023. The copyright holder for this preprint (which was not certified by peer review) is the author/funder, who has granted bioRxiv a license to display the preprint in perpetuity. It is made available under aCC-BY-NC 4.0 International license.

ON attractor that results from providing NO under ambient CO_2 and Figure *6*D illustrates the mechanism through which providing NO can lead to closure. In agreement with the model predictions, it was observed experimentally that provision of ROS [44] or CaIM (Ca^{2+} influx through the membrane, which is equivalent to providing external Ca^{2+}) [19] results in closure under ambient CO_2. The predicted closure-inducing effect of additional interventions is supported by experimental evidence, e.g. NO [51, 52], cADPR [54], 8-nitro-cGMP [53] were shown to induce closure as a signaling element of the ABA-induced closure network.

Experimental validation of model predictions

Our model predicts that the activation of the MSM is an important part of the process of stomatal closure both in ambient and high CO_2 (see Figure 5A and Figure *6*D). A follow-up conclusion from this prediction is that earlier activation of the MSM would lead to earlier closure. One of the nodes whose constitutive activity is predicted to activate the MSM and lead to closure in ambient CO_2 is NO. In our model, applying NO under high CO_2 activates the MSM sooner. Hence, supplying NO is predicted to cause hypersensitivity of closure under high CO_2 (i.e., faster high CO_2-induced closure). To assess the validity of this prediction, we experimentally tested the effect of NO on high CO_2 response by applying SNP (sodium nitroprusside dihydrate), an NO donor (Figure *7*A, see Methods for experimental assay description). To observe any speed-up of the closure process, we used short treatments (10 and 20 minutes). We found that under high (800 ppm) CO_2, the stomatal aperture under SNP treatment (orange and grey bars) is significantly lower than that without SNP treatment (blue bars, p=3.0e-2, Student's t-test). Furthermore, the mean aperture corresponding to the 10 min combined treatment of 0.15 mM SNP and high CO_2 is lower than the mean aperture corresponding to the 20 min high CO_2 treatment (rightmost blue bar, p=4.3e-2, Student's t-test), indicating that SNP treatment speeds up the high CO_2 induced closure process, consistent with our model prediction.

bioRxiv preprint doi: https://doi.org/10.1101/2023.10.23.563079; this version posted October 25, 2023. The copyright holder for this preprint (which was not certified by peer review) is the author/funder, who has granted bioRxiv a license to display the preprint in perpetuity. It is made available under aCC-BY-NC 4.0 International license.

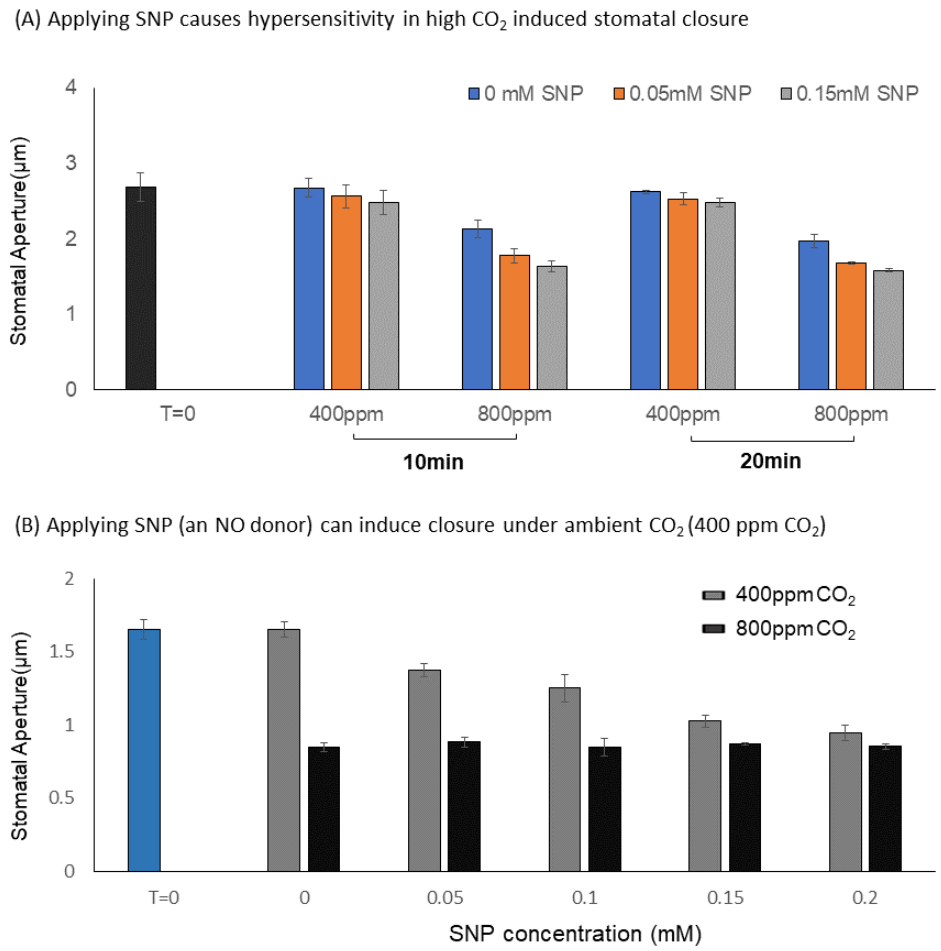

Figure 7 Experimental validation of the predicted closure responses when applying NO (via the NO donor sodium nitroprusside dihydrate, SNP) in ambient or high CO_2. (A) As predicted by the model, applying SNP causes hypersensitivity in high CO_2 induced stomatal closure: the combined treatment (orange and grey bars) leads to a lower mean aperture than high CO_2 alone (blue bars), and a 10 min combined treatment leads to a lower mean aperture than a 20 min treatment of high CO_2 alone. (B) Applying SNP (NO donor) under ambient (400 ppm) CO_2 induces closure in a dose-dependent manner (grey bars), as predicted. The highest concentration of SNP yields a similar degree of closure as high (800 ppm) CO_2 (black bars). The bars indicate the mean ± SE aperture size from at least three independent experiments with 30-40 apertures measured per treatment.

Furthermore, we experimentally validate the prediction that NO can induce closure under ambient CO_2. Our model predicts that under ambient CO_2, NO can still activate the MSM, consequently inducing closure (Figure *4*C, Figure *6*D). Previously, NO has been shown to induce closure as a signaling element of the ABA induced closure network [51, 52]. Yet, it has been unknown whether the degree of NO induced closure (aperture reduction) is comparable to high CO_2 induced closure. We found that applying the NO donor SNP under ambient CO_2 can indeed induce stomatal closure (Figure *7*B, grey bars), as predicted by our model. The reduction in aperture caused by 0.2 mM SNP is statistically significant (p=6.9e-4, Student's t-test), and close to the

bioRxiv preprint doi: https://doi.org/10.1101/2023.10.23.563079; this version posted October 25, 2023. The copyright holder for this preprint (which was not certified by peer review) is the author/funder, who has granted bioRxiv a license to display the preprint in perpetuity. It is made available under aCC-BY-NC 4.0 International license.

reduction in aperture caused by CO_2 of 800 ppm (black bars). This result confirms the model prediction that NO can induce closure in ambient CO_2.

Taken together, these experiments not only validate our model predictions regarding the effects of NO, but also support the model-predicted importance of the main stable motif.

Stable motif analysis predicts a new regulatory relationship between NO and ABI2

Analysis of the inconsistencies between the model's results and experimental observations can identify edges that are missing from the network model. The node NO offers an example of this kind as well. For example, while our model recapitulates NO-induced closure in ambient CO_2, it does not capture the observation that NO depletion leads to loss of stomatal closure under elevated CO_2 [22]. This discrepancy suggests that there is a not-yet-known regulatory effect of NO that makes it necessary for a closure mechanism. This unidentified regulatory effect of NO can be predicted from our stable motif analysis. In our current model under high CO_2 and NO KO, the Main Stable Motif can still lock-in by the activation of its driver, the inactivity of HT1, thus leading to a closure ON attractor (Figure 8A, Figure *4*D). According to current knowledge, NO participates in the pathway that leads to calcium influx from intracellular stores into the cytosol (CIS) [62]. Disruption of this pathway eliminates one mechanism of increasing the cytosolic Ca^{2+} level, but it does not perturb the Main Stable Motif. To be able to drive the system away from a closure ON attractor, NO KO should prevent the lock-in of the Main Stable Motif from activating closure (Figure 8B). Thus, we hypothesize that NO regulates at least one of the nodes in the MSM, namely, it activates ROS, RbohD/F, or OST1 minimum function, or inhibits ABI1, ABI2, or HAB1. Indeed, we experimentally found that NO inhibits ABI2's phosphatase activity (Figure 8C, and see Methods). This result suggests that the mechanism (or one of multiple contributing mechanisms) leading to impairment of stomatal closure under NO knockout could be the increase of ABI2's activity, which obstructs the minimal functional OST1 activity and precludes the lock-in of the MSM. As a decrease of ABI2's phosphatase activity makes the activation of the MSM easier, this newly-discovered inhibitory regulation likely contributes to NO-induced stomatal closure as well. The experimental confirmation of this stable-motif-based model prediction highlights the power of our model in predicting/prioritizing potential regulatory relationships and understanding the mechanisms of signal transduction.

bioRxiv preprint doi: https://doi.org/10.1101/2023.10.23.563079; this version posted October 25, 2023. The copyright holder for this preprint (which was not certified by peer review) is the author/funder, who has granted bioRxiv a license to display the preprint in perpetuity. It is made available under aCC-BY-NC 4.0 International license.

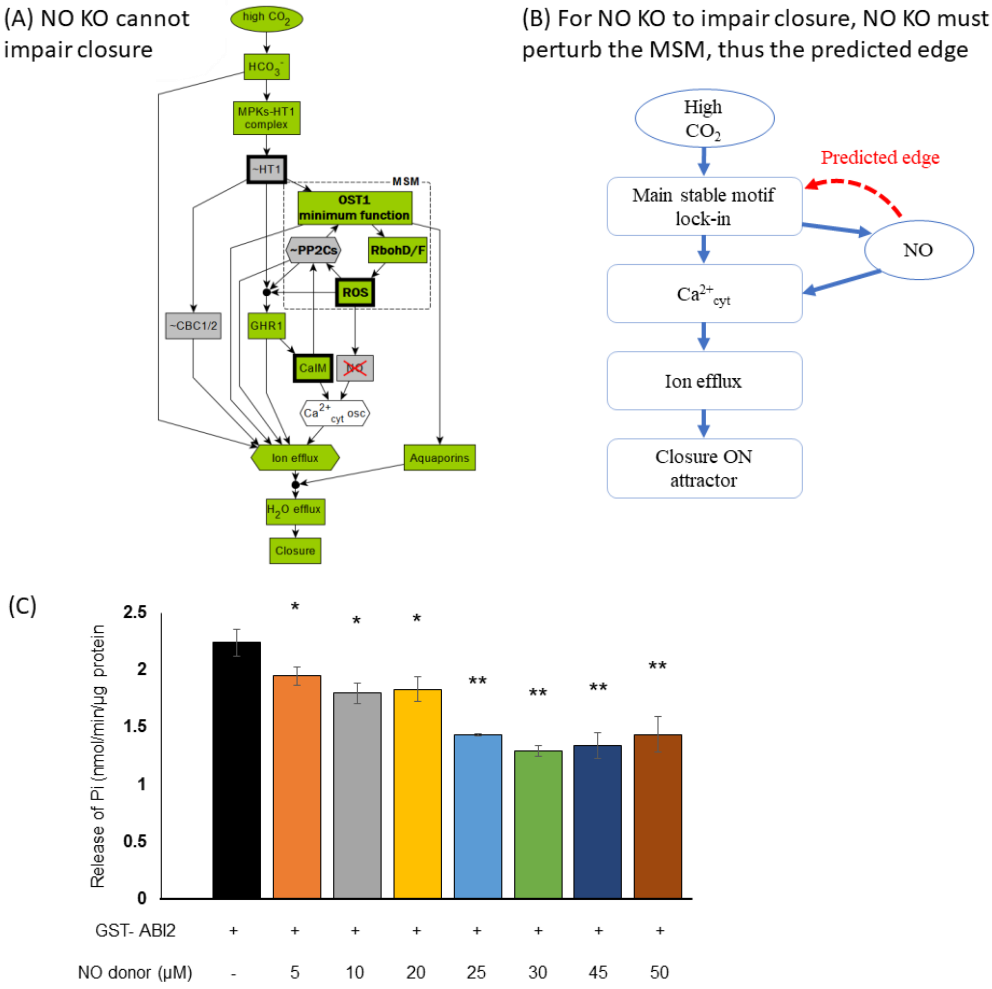

Figure 8. Network-based analysis predicted a new regulatory edge between NO and PP2Cs, which was validated by experiment. (A) Logic diagram showing that high CO_2 can activate closure despite NO KO; (B) Conceptual sketch of NO's role in the network and the predicted edge. NO must regulate the Main Stable Motif, otherwise loss of NO cannot impair high CO_2 induced closure. (C) Experimental validation showing NO inhibits ABI2 phosphatase activity. The y axis shows the effect of increasing concentrations of the NO donor SNP on ABI2 activity, quantified by measuring the amount of phosphate released from a phosphopeptide substrate, as described in Methods. The bars indicate the means ± SE of three biological replicates. Significant differences between phosphatase activity of ABI2 alone and ABI2 treated with NO donor are indicated (**P < 0.001, *P < 0.05, Student's t-test).

Our model predicts which nodes of the high CO_2 signaling network could be potential targets of currently unconnected nodes

There are signaling elements that are convincingly implicated in CO_2 signaling, yet their connection to the signaling network remains unknown. During our literature review and data curation process, we placed such elements into the "insufficient connection" category. For example, *big1* mutants are compromised in elevated CO_2-

bioRxiv preprint doi: https://doi.org/10.1101/2023.10.23.563079; this version posted October 25, 2023. The copyright holder for this preprint (which was not certified by peer review) is the author/funder, who has granted bioRxiv a license to display the preprint in perpetuity. It is made available under aCC-BY-NC 4.0 International license.

induced stomatal closure and bicarbonate activation of S-type anion channel currents [63], yet BIG1's connection to known guard cell signaling elements remains undiscovered. Connecting these elements to the existing CO_2 network can improve understanding of guard cell CO_2 signaling and could lead to testable predictions. Our model offers a way to identify and prioritize potential targets of these unconnected elements based on the effects of node perturbations (Figure *6*). The idea is that, if a node perturbation yields a similar response in the model to the observed effect of the unconnected signaling element, the node is then a potential target of the signaling element. For example, the *big1* mutant is known to have impaired CO_2-induced closure. Our model simulations (Figure *6*A) yield a comprehensive list of 24 single node perturbations that could impair closure. We predict that the *big1* mutant regulates one of these nodes; any alternative single target of *big1* would not cause loss of closure in the model. Moreover, one can utilize additional evidence to further narrow down the target candidates. For example, as *big1* mutants are also compromised in bicarbonate activation of S-type anion channel currents, we can further filter the 24 candidate nodes to those that satisfy both conditions: (1) the node is downstream of bicarbonate; and (2) the node's perturbation results in reduced SLAC1 activity (reflected by the node AnionEM, which incorporates the effect of both SLAC1 channel nodes). This filter narrows the list of potential targets of BIG1 to 9 nodes, namely, MPKs, ABI1, ABI2, GHR1, HT1, OST1 minimum function, RbohD/F, and ROS. One can design experiments to test if some of these nodes are indeed perturbed in *big1* mutants. If a broader pool of candidate targets is needed, one could also consider the nodes whose perturbations causes hyposensitivity in high CO_2 induced closure (five nodes in the last row of Table 3). These nodes may be appropriate because it might be difficult to distinguish reduced sensitivity and hyposensitivity in experiments.

Table 3 Model-predicted potential regulation targets to impair high CO_2 induced closure. If a knockout of a signaling element impairs high CO_2 induced closure, the model predicts the knockout will perturb one of these nodes. The first three rows are categorized based on the network location of the node, i.e., which component it is in. The last row is an extension where we hypothesize that perturbations causing hyposensitivity in the model could also be considered as having the potential to impair closure. Bold font indicates an example of 9 prioritized targets for BIG1, which are downstream of bicarbonate and whose perturbation can also cause reduced SLAC1 activity, as observed in the *big1* mutant.

Category	Potential regulation target to impair closure
High CO_2 in-component or source node (6 nodes)	CA14, CO_2 porins, CO_2 entry of cell, HCO_3^-, **MPKs, NADPH**
Signal transduction SCC (10 nodes)	**ABI1**, **ABI2**, Ca^{2+}_{cyt}, Ca^{2+}ATPase, **GHR1**, **HT1**, **OST1 minimum function**, **RbohD/F**, **ROS**
Ion Channel out-component (8 nodes)	H^+ ATPase, Anion EM, Aquaporins, Depolarization, H_2O Efflux, K^+ efflux, KEV, KOUT
Nodes/perturbations causing hyposensitivity (5 nodes)	CaIM, CBC1/2, MPKs-HT1complex, QUAC1, SLAC1 CO_2

bioRxiv preprint doi: https://doi.org/10.1101/2023.10.23.563079; this version posted October 25, 2023. The copyright holder for this preprint (which was not certified by peer review) is the author/funder, who has granted bioRxiv a license to display the preprint in perpetuity. It is made available under aCC-BY-NC 4.0 International license.

By a similar logic, the "hypersensitivity" response category in Figure 6A allows target prediction for signaling elements whose perturbation (knockout or constitutive activation) promotes closure. For example, faster closure is observed in plants lacking the ABC transporter AtABCB14 [64]. Hence, our model predicts that the knockout of AtABCB14 causes a node perturbation that leads to hypersensitivity, as annotated in Figure *6*A. Furthermore, one can predict/prioritize targets of a signaling element as those that can induce closure in ambient CO_2, based on the node perturbations that can include closure in ambient CO_2 (Figure *6*C). To summarize, our model provides ways to prioritize potential targets to link previously unconnected nodes with the high CO_2 signaling network. Importantly, we only used BIG1 and AtABCB14 as examples; the proposed prediction method is general.

III. Discussion

In this work we constructed a signaling network that integrates current information regarding the signaling mechanisms underlying high CO_2 induced stomatal closure in guard cells. We assembled the nodes and edges of the network model from a thorough literature review process, with rigorous definitions of which signaling elements are involved in CO_2 signaling and which are not; we also deployed a multi-node presentation to capture multiple mechanisms of the same element. Finally, we conducted a comprehensive model performance evaluation, making sure that our model indeed has high consistency with experimental observations. A previous model by Schroeder and colleagues of ABA and high CO_2 induced closure, constructed as a case study of the Boolink graphical user interface [29], added to a model we originally created for ABA-induced stomatal closure [3] six nodes (CO_2, CA1, CA4, MPK4/12, HT1, CBC1/CBC2) and changed five functions (GHR1, CaIM, $Ca^{2+}{}_c$, Microtubule, H_2O efflux) without comprehensive evaluation of the model's accuracy in recapitulating all experimental observations regarding high CO_2 induced closure. In fact, two of the additions make the rest of the network superfluous: specifically, the function that controls CaIM has "OR CO_2" in it, which means that high CO_2 induces CaIM regardless of the rest of the regulators of CaIM; the function of H_2O efflux also has "OR CO_2" in it, which makes water efflux happen directly in response to CO_2 regardless of the rest of the regulators of aquaporins. The combined effect of these two assumptions results in closure. In other words, the model of Karanam et al. short-circuits essentially the entire CO_2 signaling network by making CO_2 directly activate the very downstream part of the network. As a result, the model will not be able to capture the experimentally observed responses to many perturbations in the signaling network, e.g. the impaired high CO_2 induced closure under *slac1*1 [47], *ht1-2* [10] and *mpk4/mpk12* [12] mutants. By comparison, a rigorous model construction process allows our CO_2 model to comprehensively reproduce experimental observations related to high CO_2 induced closure.

Network methodologies reveal key decision-making motifs, pinpoint driver nodes, elucidate signal transduction mechanisms, predict new edges and responses

bioRxiv preprint doi: https://doi.org/10.1101/2023.10.23.563079; this version posted October 25, 2023. The copyright holder for this preprint (which was not certified by peer review) is the author/funder, who has granted bioRxiv a license to display the preprint in perpetuity. It is made available under aCC-BY-NC 4.0 International license.

Our network-based modeling framework integrates piece-wise (node to node) biological knowledge to form a high-level comprehensive view of the signal transduction network underlying high CO_2 induced stomatal closure. This framework complements conventional biological approaches that often focus on single regulators or single pathways. Our analysis supports recent findings that HT1 is a key decision-making node of the CO_2 signaling system [13, 14], and offers additional insights regarding the ambient CO_2 setting: closure induced by, e.g., exogenous ROS or Ca^{2+} in ambient CO_2 must involve the inactivation of HT1 and the activation of a positive feedback loop (the Main Stable Motif, formed by ROS, OST1 and the PP2Cs). Conversely, under conditions that activate HT1 the nodes of this positive feedback loop may also lock-in to their opposite states and lead to closure OFF.

We have also introduced the concept of logic diagrams to visually depict the logical implications of events in the closure process, highlighting key nodes and pathways (subgraphs) responsible for decision-making of the system. The logic diagrams explain not only how signal transduction leads to stomatal closure under high CO_2, but also how closure is lost or restored. Leveraging these concepts, we explain the mechanisms behind the five types of simulated closure responses in the presence of perturbations.

Combining these network-based methodologies allows the generation of model predictions that lead to novel experimental findings. It is important to note that the inconsistencies between of the model and experimental results also yield insights. For example, we found that the model is incapable of reproducing the experimental observation that NO knockout impairs high CO_2 induced closure; by understanding that this inconsistency results from the NO-independent lock-in of the Main Stable Motif, we predicted that NO must regulate the MSM, and successfully validated this prediction experimentally, showing that NO inhibits ABI2, one of the PP2Cs in the MSM.

Unexplained mechanisms in CO_2 signaling

There are signaling elements known to mediate closure in response to a certain signal, but understudied in CO_2 signaling; for example, PA (Phosphatidic acid). In our model construction process, when we designate each piece of knowledge regarding the regulation of a node by another into one of the five categories (see Supporting Info S1 and Table *1*), we place such elements into the "generic", or "insufficient evidence" categories. This way, our categorization of evidence can prioritize experiments to explore the roles of signaling elements in the context of CO_2 signaling.

Our model construction and validation process included the examination of multiple different hypotheses regarding the role of certain nodes in high CO_2 signaling. For example, the role of RHC1 in CO_2 signaling is under debate: while Tian et al. showed experimental evidence that RHC1 is an essential CO_2 signaling component [15], Tõldsepp et al. observed that a different *rhc1* mutant shows no reduction of high CO_2-induced closure. We tested both versions of the HT1 regulatory function, with and without RHC1, and found that the function without RHC1 has a higher accuracy in capturing experimental observations. Therefore, we adopt the HT1 function without RHC1, more consistent with [16]. Our interpretation is that RHC1's regulatory effect

bioRxiv preprint doi: https://doi.org/10.1101/2023.10.23.563079; this version posted October 25, 2023. The copyright holder for this preprint (which was not certified by peer review) is the author/funder, who has granted bioRxiv a license to display the preprint in perpetuity. It is made available under aCC-BY-NC 4.0 International license.

on HT1 is weaker than that of MPKs, thus it is insufficient to include in a Boolean model.

Some CO_2 signaling mechanisms remain unclear. For example, observations about guard cell cytosolic pH suggests undiscovered buffering capacity in the cytosol. Brearley et al. and Xue et al. [8, 30] observed that cytosolic pH does not increase under high CO_2 induced closure. On the other hand, after CO_2 enters the guard cell, it undergoes the chemical reaction $CO_2 + H_2O \rightarrow HCO_3^- + H^+$ catalyzed by CA1/4, producing H^+. So, there must be some buffering capacity or other mechanism to keep cytosolic pH constant. Understanding this mechanism may affect other components in the network, and its refinement may improve the model as well as our understanding of the high CO_2 signaling mechanism.

Future discovery of new signaling elements and interactions that participate in high CO_2 induced closure will call for updates of this model, including the addition of new nodes and/or new edges, the possible removal of assumed edges (shown as dotted lines in Figure 1), or changes to the regulatory functions of certain nodes. It is important to note that even when new signaling elements and interactions are incorporated into the CO_2 model, certain structural and dynamic features of the model will be preserved. For example, the network will still have a strongly connected component (see Figure 1B) that includes at least the 20 nodes currently in it. The updates will be such that the model preserves the current model's agreements with experimental results. The coupling of the structural and dynamical preservation means that the decision-making role of the main stable motif will also be maintained in the updated model, even if newly added edges will increase its size (for example, by NO joining it). It is likely that newly discovered interactions will support the regulatory relationships that drive the decisions of the system. For example, the inhibition of ABI2 by NO is an additional mechanism by which NO contributes to the activation of the MSM. Ultimately, a cycle between experimental and modeling approaches offers the most effective way to elucidate the full network of high CO_2 induced closure.

IV. Methods and Data

Construction of the CO_2-signaling network and dynamic model

As described in the main text, we extract regulatory relationships from the literature (Supporting Info S1), and compile them into nodes and edges of the network (Supporting Info S2). Then we construct the regulatory functions (Supporting Info S3) based on the regulatory relationships.

Simulation settings of the dynamical model

In simulation, we initialize the *in silico* stomata in a pre-stimulus open state, with closure-inhibiting nodes ON (namely ABI1, ABI2, HAB1, HT1, and H^+ ATPase) and other nodes OFF (see SI S4 for complete initial condition). For example, Anion Efflux, a node that becomes activated during high CO_2-induced closure, is initialized in the OFF state. We deploy a discrete-time simulation, with stochastic random order asynchronous update: at each discrete round of updates (or timestep), all nodes are

bioRxiv preprint doi: https://doi.org/10.1101/2023.10.23.563079; this version posted October 25, 2023. The copyright holder for this preprint (which was not certified by peer review) is the author/funder, who has granted bioRxiv a license to display the preprint in perpetuity. It is made available under aCC-BY-NC 4.0 International license.

updated in a randomly selected order. A different order is generated in each timestep. The main advantage of random order asynchronous update is that it can capture consensus dynamics without implementation of exact timing, as the actual timing and durations of the processes happening in the system are typically unknown. The stochasticity of the update helps avoid spurious behaviors that depend on synchrony (i.e., which only appear under synchronous update, where all nodes are updated at the same time, which is biologically unrealistic). We perform this simulation for 30 timesteps, long enough for the system to reach its attractor (stable long-time behavior). In this way, we can simulate how a node's state changes over time during the stomatal closure process.

We perform 1000 replicate simulations, i.e., 1000 "*in silico* stomata" simulations, then calculate the "percentage of node activation" at each timestep as our metric, meaning the percentage of simulations in which the node (e.g. Closure) is in state 1/ON. For example, if 1000 replicate simulations yield 510 cases where closure is ON at time step 30, the simulated percentage of closure is 51%. In this way, oscillations and multistability with different node states will display a percentage of node activation value between 0% and 100%.

Stable motif and attractor analysis

Stable motifs are the smallest strongly connected components in a system that can sustain a unique steady state for the constituent nodes [26, 55]. Stable motifs are identified in an expanded representation of the network (which includes the network's regulatory functions as part of the network structure). A weaker version of a stable motif, called a conditionally stable motif [56], can sustain a unique steady state for its nodes as long as certain node(s) that regulate the motif are in a specific fixed state. The stable motifs and conditionally stable motifs of a Boolean network determine its attractors: one can uniquely associate sequences of stable motifs (stabilized in the order given by the sequence) to each attractor.

A driver (or driver set) of a stable motif is the node (or node combination) and its state that, when kept fixed, eventually leads to the locking in of the stable motif after sufficient updates. We used the python library pystablemotifs [27] to analyze the stable motifs, attractors and their control methods. The library is available through the github page https://github.com/jcrozum/pystablemotifs.

Validation against experimental observations

We use the experimental observations in Supporting Info S1 that were not used in model construction (a subset of the indirect regulations, marked as "V" for validation in Supporting Info S1) as the ground truth for model validation. Because quantifying the (reduction of) stomatal aperture is difficult in both experiment and Boolean model, when comparing the experiment-based expected outcomes with the model simulation results, we employ a lenient criterion for consistency: any model-predicted defect (i.e. node percentage < 100%) is considered qualitatively consistent with either reduced response or no response. For example, if a simulation yields a closure percentage = 0.5,

bioRxiv preprint doi: https://doi.org/10.1101/2023.10.23.563079; this version posted October 25, 2023. The copyright holder for this preprint (which was not certified by peer review) is the author/funder, who has granted bioRxiv a license to display the preprint in perpetuity. It is made available under aCC-BY-NC 4.0 International license.

then it is considered consistent with both "reduced closure" and "no closure" in experimental observation. This type of consistency criterion was used in previous modeling as well [3]. We provide the comprehensive validation results in Supporting Info S4. The supplementary file also includes the trivially consistent cases due to circular reasoning, denote "true by construction". For example, bicarbonate-induced activation of S-type anion channels was reduced in the dominant active *abi1* mutants (ABI1 CA) [43], but because ABI1 is a input in both SLAC1 functions and ABI1 ON is sufficient to deactivate both SLAC1 nodes, this experimental observation is captured by model/rule construction, and calling it a validation would be circular reasoning. This type of validation is not counted in our assessment of model accuracy performance.

Definition of the response categories in CPC values, for simulated knockout or constitutive activity

We defined the cumulative percentage of closure (CPC) as the sum over 30 timesteps of the fraction of simulations that have the closure node in state 1 (ON), over 1000 replicate simulations. Thus, CPC ranges from 0 (if the percentage of closure were 0% at every time step) to 30 (if the percentage of closure were 100% at every time step). The CPC metric helps capture time-sensitive behavior such as hypo-/hyper-sensitivity, reflected as a small CPC difference from wildtype CPC.

We define the five categories of responses based on the CPC value and attractor state: close to wildtype, hypersensitivity, hyposensitivity, reduced closure, and no closure. We define the wildtype response range from the default high CO_2-induced closure response. Since the simulation is stochastic (i.e. the CPC value can be different for each simulation), we determine the default CPC range by 600 batches of 1000 replicate simulations under the default high-CO_2 signal, and define its CPC range as the "close to wildtype" CPC range (20.405 to 20.709). CPC values above this range are classified as hypersensitivity, meaning that the stomata reach the closure state significantly faster than wildtype. CPC values below the wildtype range with 100% percentage closure at the final timestep are classified as hyposensitivity. Reduced closure is the CPC value being much lower than wildtype range, with the final percentage of closure being between 0 and 1. In all of the observed cases in this last category, the closure value is oscillating in the attractor. Lastly, no closure is defined as the CPC value being zero or very close to zero, with final percentage of closure being zero. A small positive CPC can occur here, because closure may temporarily turn ON during the response process, though it cannot be maintained. The comprehensive CPC simulation results are provided in Supporting Info S6.

Logic diagrams of the CO_2 network model

The logic diagram is an integration of the network and node states that yields a specific outcome (e.g., the ON state of the node Closure). It is an expansion of the concepts of elementary signaling mode [57] and logical domain of influence [58], both of which are subgraphs of the expanded network (also called logical hypergraph), which incorporates the Boolean functions of all the nodes in the network [55]. The logic diagram indicates the node states visually: nodes whose name is preceded by ~ and

bioRxiv preprint doi: https://doi.org/10.1101/2023.10.23.563079; this version posted October 25, 2023. The copyright holder for this preprint (which was not certified by peer review) is the author/funder, who has granted bioRxiv a license to display the preprint in perpetuity. It is made available under aCC-BY-NC 4.0 International license.

have grey background are inactive, nodes with green background are active, and nodes whose name is followed by "osc" and have a white background oscillate. A single edge in a logic diagram represents a sufficient regulatory relationship that can achieve the indicated state of the target node; multiple edges incident on the same black dot represents "AND" logic, indicating that all nodes are required to achieve the target node state. A logic diagram may condense fully linear pathways of nodes and edges in the original network, to simplify visualization. This type of condensation does not change the regulatory logic of the network model [59].

To better help visual parsing in the CO_2 network model, we also merged a few nodes of the original network. The node "PP2Cs" merges three members of the PP2C protein family, because these nodes have identical regulation. The technical definition of the merged node is PP2Cs = ABI1 or ABI2 or HAB1. The node "Ion flow" merges AnionEM and K^+ efflux (i.e, Ion flow = AnionEM and K+ efflux). We also use a single node "Ca^{2+}_{cyt} osc" to represent the Ca^{2+}_{cyt} - Ca^{2+} ATPase negative feedback cycle, capturing the oscillating behavior of Ca^{2+}_{cyt} in the presence of a Ca^{2+} source (CaIM or CIS) and due to the inhibitory effect of the Ca^{2+} ATPase. We use hexagonal symbols for "PP2Cs" and "Ion efflux" as they represent a node set (Figure 5). Note the "Ion efflux" hexagon node needs multiple incident edges to activate, causing an exception of the edge definition.

The logic diagram can be read as a sequence of events and the conditions necessary for these events. For example, the sequence of events necessary for high CO_2 induced closure described by Figure 5A is the following: high CO_2 activates HCO_3^-, which inactivates HT1 via the formation of the MPKs-HT1 complex. HT1 being OFF then activate OST1 minimum function, which eventually activates the MSM. The simultaneous activation of the MSM and inactivation of HT1 (indicated by the black dot) activates GHR1, which in turn activates CPKs. GHR1 activates CaIM, which leads to cytosolic Ca^{2+} transients or oscillations. The MSM, GHR1, Ca^{2+}_{cyt}, HCO_3^-, as well as the inactivity of CBC1/2 contribute to the activation of Ion flows. The simultaneous activation of Ion flows and OST1-activated Aquaporin yield H_2O efflux, which then leads to Closure. As another example, the logic diagram in Figure *6*D shows that the activation of the MSM (e.g., by CaIM) leads to CIS, which then leads to cytosolic Ca^{2+} transients or oscillations, which activate MPK activity, which inhibits HT1, which then allows the activation of GHR1, then of the generic SLAC1 node, and finally the activation of the node Closure.

Plant materials and growth conditions

Arabidopsis thaliana Columbia (Col-0) accession plants were used as wild-type. Col-0 were germinated on MS agar plates for 2 weeks and then grown in soil (1:1 mixture of Metro Mix 360: Sunshine Mix LC1 (Sun Gro Horticulture) in a growth chamber with an 8-h-light/16-h-dark cycle, 120 µmol photons m^{-2} s^{-1} light, and 20°C. Young fully expanded leaves from 4-5-week-old plants were used for stomatal aperture assay experiments.

bioRxiv preprint doi: https://doi.org/10.1101/2023.10.23.563079; this version posted October 25, 2023. The copyright holder for this preprint (which was not certified by peer review) is the author/funder, who has granted bioRxiv a license to display the preprint in perpetuity. It is made available under aCC-BY-NC 4.0 International license.

Stomatal aperture assay

Stomatal apertures were assayed as described previously with slight modifications [65]. In brief, epidermal peels were hand-peeled from the abaxial surfaces of leaves and then were floated interior-side down on an opening solution (20 mM KCl, 10 mM MES-KOH pH 6.15, 50 µM $CaCl_2$) under white light (150 µmol m^{-2} sec^{-1}) for 3 h to induce maximum opening of the stomata (initial aperture). After the 3h preincubation period, epidermal peels were floated in a six-well plate (each well with a diameter of 35 mm and height of 17 mm) containing pre-equilibrated high (800 ppm) or ambient (400 ppm) CO_2 opening solution (approximately 3 mL). Subsequently, the multiwell cell culture plate was placed in a petri dish chamber and sealed with parafilm. The high or ambient CO_2 concentration was continuously maintained within the chamber using a Licor-6400 (flow rate of 500 µmol s^{-1}) while the samples were further incubated under white light (150 µmol m^{-2} sec^{-1}). After 3 hr of incubation, the epidermal peels were imaged with a 40X objective using a light microscope (Nikon Diaphot 300) coupled to a digital camera (Nikon Coolpix 990). Stomatal apertures were measured in each image using ImageJ. To determine the effects of NO donor SNP (sodium nitroprusside dihydrate; Sigma 71778) on CO_2-induced stomatal closure, experiments were performed according to the method described by [66] with some modifications. Briefly, epidermal peels were incubated for 3 hr in the opening buffer to induce stomatal opening. Subsequently, the epidermal peels were transferred to the opening buffer without or with SNP at the indicated concentrations and then treated under ambient CO_2 (400 ppm CO_2) or elevated CO_2 (800 ppm CO_2) in light for the indicated durations. A total of 30-40 stomatal apertures were measured per treatment for each individual experiment. Data presented are the mean of 3 independent experiments.

Phosphopeptide-based phosphatase activity assay

To examine the effect of NO donor on ABI2 phosphatase activity, GST-tagged ABI2 was heterologously expressed in *Escherichia coli* and subsequently purified as described [67] with minor modifications. Briefly, pDEST15-ABI2 was constructed by transferring *ABI2* cDNA from pCR8/GW/TOPO TA vector to the N-terminal GST fusion expression vector pDEST15 (Invitrogen) by Gateway LR recombination (Invitrogen). The cloned construct was verified by sequencing. The GST-ABI2 protein was expressed in *E. coli* BL21(DE3) pLysS Rosetta cells by induction with 0.5 mM IPTG for 16 hr at 16 °C. The cells were harvested by centrifugation (6000 g, 8 min, 4°C) and stored at -80°C until use. All purification procedures were carried out at 4 °C. The final cell pellet was resuspended in 10 ml of B-PER reagent (Pierce, catalog number 78243) supplemented with 1 mg/ml lysozyme (Sigma, catalog number L6876), 25 mg/ml DNAse and EDTA-free complete protease inhibitor (Thermo Fisher scientific, catalog number A32955) and incubated for 60 min at 4 °C with gentle shaking. The cell lysate was spun at 16000g for 15 min. at 4 °C and the resulting supernatant was filtered using a 0.45 µm filter. Subsequently, the supernatant was loaded onto a 5 ml QIAGEN polypropylene column packed with GST glutathione agarose resin (Pierce, 16100) and the column-bound protein was eluted with

bioRxiv preprint doi: https://doi.org/10.1101/2023.10.23.563079; this version posted October 25, 2023. The copyright holder for this preprint (which was not certified by peer review) is the author/funder, who has granted bioRxiv a license to display the preprint in perpetuity. It is made available under aCC-BY-NC 4.0 International license.

equilibration buffer (25 mM Tris-HCl pH 7.5, 150 mM NaCl) supplemented with 20 mM reduced L-glutathione (Sigma, catalog number G4251). The purity of the recombinant GST-ABI2 was estimated by analysis of aliquots separated on a 12% SDS polyacrylamide gel stained with Gel-Code Blue (Thermo), and the concentration was estimated based on known concentrations of Fraction V BSA (Pierce, catalog number 23209) run on the same gel.

The effect of NO donor on ABI2 phosphatase activity was carried out using the Ser/Thr phosphatase assay kit (Promega; catalog number V2460). The reaction was performed in a 50 µl volume containing 28 nM of purified recombinant GST-ABI2 protein in the presence or absence of the indicated concentration of NO donor SNP. After 30 min incubation at 30 °C, the reaction was stopped by addition of 50 µl of molybdate dye/additive solution. The resulting mix was incubated for another 20 min at room temperature followed by absorbance measurements at 630 nm in a Synergy Neo2 multimode plate reader (Biotek). The amount of released phosphate was calculated based on a standard curve obtained using phosphate standard solutions of known concentration.

Acknowledgements

The authors thank Dr. David Chakravorty, Dr. Yotam Zait, Dr. Ángel Ferrero-Serrano, and Dr. Jordan C. Rozum for helpful discussions.

Supporting Information files

S1 Table. Summary of evidence from our literature review for CO_2 network and model construction.

S2 Table. Description of the 47 nodes and 95 edges of the CO_2 network

S3 Text. Regulatory functions of the dynamic model and their justifications

S4 Text. Supporting Information on signaling elements whose participation in CO_2 signaling has not been tested and on minor conditionally stable motifs in the CO_2 network.

S5 Table. Comparison of the model simulation results with experimental observations

S6 Table. CPC results of systematic perturbation (KO/CA) simulations under high CO_2 and ambient CO_2

Competing interests

The authors declare that no competing interests exist. The authors do not have a related or duplicate manuscript under consideration (or accepted) for publication elsewhere. This study does not involve human or animal research ethics.

Financial Disclosure Statement

bioRxiv preprint doi: https://doi.org/10.1101/2023.10.23.563079; this version posted October 25, 2023. The copyright holder for this preprint (which was not certified by peer review) is the author/funder, who has granted bioRxiv a license to display the preprint in perpetuity. It is made available under aCC-BY-NC 4.0 International license.

This work was supported by NSF grant MCB 1715826 to S.M.A. and R.A. Link: https://www.nsf.gov/awardsearch/showAward?AWD_ID=1715826. The funders had no role in study design, data collection and analysis, decision to publish, or preparation of the manuscript.

Data Availability

Data in this study are provided in the Supporting Information files.

Author contributions

Conceptualization: Xiao Gan, Reka Albert, Sarah M. Assmann.

Data curation: Xiao Gan, with input from all authors.

Formal analysis: Xiao Gan, Kyu Hyong Park.

Funding acquisition: Reka Albert, Sarah M. Assmann.

Investigation: All authors.

Methodology: Xiao Gan, Palanivelu Sengottaiyan, Kyu Hyong Park, Reka Albert.

Project administration: Reka Albert, Sarah M. Assmann.

Software: Xiao Gan, Kyu Hyong Park.

Supervision: Reka Albert, Sarah M. Assmann.

Validation: Palanivelu Sengottaiyan, Xiao Gan.

Visualization: All authors.

Writing: Xiao Gan, Reka Albert, and Sarah M. Assmann, with input from all authors.

References

1. Assmann, S.M. and T. Jegla, *Guard cell sensory systems: recent insights on stomatal responses to light, abscisic acid, and CO.* Curr Opin Plant Biol, 2016. **33**: p. 157-167.
2. Hsu, P.K., et al., *Signaling mechanisms in abscisic acid-mediated stomatal closure.* Plant J, 2021. **105**(2): p. 307-321.
3. Albert, R., et al., *A new discrete dynamic model of ABA-induced stomatal closure predicts key feedback loops.* PLOS Biology, 2017. **15**(9): p. e2003451--e2003451-.
4. Munemasa, S., et al., *Mechanisms of abscisic acid-mediated control of stomatal aperture.* Current Opinion in Plant Biology, 2015. **28**: p. 154-162.
5. *Dr. Pieter Tans, NOAA/GML (gml.noaa.gov/ccgg/trends/) and Dr. Ralph Keeling, Scripps Institution of Oceanography (scrippsco2.ucsd.edu/).*
6. Wang, C., et al., *Reconstitution of CO2 Regulation of SLAC1 Anion Channel and Function of CO2-Permeable PIP2;1 Aquaporin as CARBONIC ANHYDRASE4 Interactor.* Plant Cell, 2016. **28**(2): p. 568-82.

bioRxiv preprint doi: https://doi.org/10.1101/2023.10.23.563079; this version posted October 25, 2023. The copyright holder for this preprint (which was not certified by peer review) is the author/funder, who has granted bioRxiv a license to display the preprint in perpetuity. It is made available under aCC-BY-NC 4.0 International license.

7. Hu, H., et al., *Carbonic anhydrases are upstream regulators of CO2-controlled stomatal movements in guard cells.* Nat Cell Biol, 2010. **12**(1): p. 87-93; sup pp 1-18.
8. Xue, S., et al., *Central functions of bicarbonate in S-type anion channel activation and OST1 protein kinase in CO2 signal transduction in guard cell.* EMBO J, 2011. **30**(8): p. 1645-58.
9. Hashimoto, M., et al., *Arabidopsis HT1 kinase controls stomatal movements in response to CO2.* Nat Cell Biol, 2006. **8**(4): p. 391-7.
10. Hashimoto-Sugimoto, M., et al., *Dominant and recessive mutations in the Raf-like kinase HT1 gene completely disrupt stomatal responses to CO2 in Arabidopsis.* J Exp Bot, 2016. **67**(11): p. 3251-61.
11. Hõrak, H., et al., *A Dominant Mutation in the HT1 Kinase Uncovers Roles of MAP Kinases and GHR1 in CO2-Induced Stomatal Closure.* Plant Cell, 2016. **28**(10): p. 2493-2509.
12. Jakobson, L., et al., *Natural Variation in Arabidopsis Cvi-0 Accession Reveals an Important Role of MPK12 in Guard Cell CO2 Signaling.* PLoS Biol, 2016. **14**(12): p. e2000322.
13. Takahashi, Y., et al., *Stomatal CO2/bicarbonate sensor consists of two interacting protein kinases, Raf-like HT1 and non-kinase-activity requiring MPK12/MPK4.* Science Advances, 2022. **8**(49): p. eabq6161.
14. Yeh, C.-Y., et al., *MPK12 in stomatal CO2 signaling: function beyond its kinase activity.* New Phytologist, 2023. **n/a**(n/a).
15. Tian, W., et al., *A molecular pathway for CO2 response in Arabidopsis guard cells.* Nature Communications, 2015. **6**(1): p. 6057.
16. Tõldsepp, K., et al., *Mitogen-activated protein kinases MPK4 and MPK12 are key components mediating CO2-induced stomatal movements.* Plant J, 2018. **96**(5): p. 1018-1035.
17. Webb, A.A.R., et al., *Carbon dioxide induces increases in guard cell cytosolic free calcium.* The Plant Journal, 1996. **9**(3): p. 297-304.
18. Young, J.J., et al., *CO(2) signaling in guard cells: calcium sensitivity response modulation, a Ca(2+)-independent phase, and CO(2) insensitivity of the gca2 mutant.* Proc Natl Acad Sci U S A, 2006. **103**(19): p. 7506-11.
19. Hubbard, K.E., et al., *Abscisic acid and CO2 signalling via calcium sensitivity priming in guard cells, new CDPK mutant phenotypes and a method for improved resolution of stomatal stimulus-response analyses.* Ann Bot, 2012. **109**(1): p. 5-17.
20. Chater, C., et al., *Elevated CO2-Induced Responses in Stomata Require ABA and ABA Signaling.* Curr Biol, 2015. **25**(20): p. 2709-16.
21. Kolla, V.A., A. Vavasseur, and A.S. Raghavendra, *Hydrogen peroxide production is an early event during bicarbonate induced stomatal closure in abaxial epidermis of Arabidopsis.* Planta, 2007. **225**(6): p. 1421-9.
22. Shi, K., et al., *Guard cell hydrogen peroxide and nitric oxide mediate elevated CO2 -induced stomatal movement in tomato.* New Phytol, 2015. **208**(2): p. 342-53.

bioRxiv preprint doi: https://doi.org/10.1101/2023.10.23.563079; this version posted October 25, 2023. The copyright holder for this preprint (which was not certified by peer review) is the author/funder, who has granted bioRxiv a license to display the preprint in perpetuity. It is made available under aCC-BY-NC 4.0 International license.

23. Li, S., S.M. Assmann, and R. Albert, *Predicting essential components of signal transduction networks: a dynamic model of guard cell abscisic acid signaling.* PLoS Biol, 2006. **4**(10): p. e312.
24. Sun, Z., et al., *Multi-level Modeling of Light-Induced Stomatal Opening Offers New Insights into Its Regulation by Drought.* PLOS Computational Biology, 2014. **10**(11): p. e1003930--e1003930-.
25. Zañudo Jorge, G.T. and R. Albert, *Cell Fate Reprogramming by Control of Intracellular Network Dynamics.* PLOS Computational Biology, 2015. **11**(4): p. 1-24.
26. Rozum, J.C., et al., *Parity and time reversal elucidate both decision-making in empirical models and attractor scaling in critical Boolean networks.* Sci Adv, 2021. **7**(29).
27. Rozum, J.C., et al., *pystablemotifs: Python library for attractor identification and control in Boolean networks.* Bioinformatics, 2021.
28. Gan, X. and R. Albert, *General method to find the attractors of discrete dynamic models of biological systems.* Physical Review E, 2018. **97**(4).
29. Karanam, A., et al., *Boolink: a graphical interface for open access Boolean network simulations and use in guard cell CO2 signaling.* Plant Physiol, 2021. **187**(4): p. 2311-2322.
30. Brearley, J., M.A. Venis, and M.R. Blatt, *The effect of elevated CO2 concentrations on K+ and anion channels of Vicia faba L. guard cells.* Planta, 1997. **203**(2): p. 145-154.
31. Savchenko, G., et al., *pH regulation in apoplastic and cytoplasmic cell compartments of leaves.* Planta, 2000. **211**(2): p. 246-255.
32. Hsu, P.K., et al., *Abscisic acid-independent stomatal CO2 signal transduction pathway and convergence of CO2 and ABA signaling downstream of OST1 kinase.* Proc Natl Acad Sci U S A, 2018. **115**(42): p. E9971-E9980.
33. Zhang, L., et al., *FRET kinase sensor development reveals SnRK2/OST1 activation by ABA but not by MeJA and high CO.* Elife, 2020. **9**.
34. Gan, X. and R. Albert, *Modeling biological information processing networks*, in *Physics of Molecular and Cellular Processes*, K.B. Blagoev and H. Levine, Editors. 2022, Springer International Publishing.
35. Jammes, F., et al., *MAP kinases MPK9 and MPK12 are preferentially expressed in guard cells and positively regulate ROS-mediated ABA signaling.* Proc Natl Acad Sci U S A, 2009. **106**(48): p. 20520-5.
36. Zhang, J., et al., *Identification of SLAC1 anion channel residues required for CO 2/bicarbonate sensing and regulation of stomatal movements.* Proc Natl Acad Sci U S A, 2018. **115**(44): p. 11129-11137.
37. Wang, R.S., A. Saadatpour, and R. Albert, *Boolean modeling in systems biology: an overview of methodology and applications.* Physical Biology, 2012. **9**(5): p. 14.
38. Kauffman, S.A., *METABOLIC STABILITY AND EPIGENESIS IN RANDOMLY CONSTRUCTED GENETIC NETS.* Journal of Theoretical Biology, 1969. **22**(3): p. 437-&.

bioRxiv preprint doi: https://doi.org/10.1101/2023.10.23.563079; this version posted October 25, 2023. The copyright holder for this preprint (which was not certified by peer review) is the author/funder, who has granted bioRxiv a license to display the preprint in perpetuity. It is made available under aCC-BY-NC 4.0 International license.

39. Naldi, A., et al., *Diversity and plasticity of Th cell types predicted from regulatory network modelling.* PLoS Comput Biol, 2010. **6**(9): p. e1000912.
40. Deritei, D., et al., *A feedback loop of conditionally stable circuits drives the cell cycle from checkpoint to checkpoint.* Sci Rep, 2019. **9**(1): p. 16430.
41. Sierla, M., et al., *The Receptor-like Pseudokinase GHR1 Is Required for Stomatal Closure.* Plant Cell, 2018. **30**(11): p. 2813-2837.
42. Webb, A.A. and A.M. Hetherington, *Convergence of the abscisic acid, CO2, and extracellular calcium signal transduction pathways in stomatal guard cells.* Plant Physiol, 1997. **114**(4): p. 1557-60.
43. Merilo, E., et al., *PYR/RCAR receptors contribute to ozone-, reduced air humidity-, darkness-, and CO2-induced stomatal regulation.* Plant Physiol, 2013. **162**(3): p. 1652-68.
44. Kwak, J.M., et al., *NADPH oxidase AtrbohD and AtrbohF genes function in ROS-dependent ABA signaling in Arabidopsis.* EMBO J, 2003. **22**(11): p. 2623-33.
45. Meyer, S., et al., *AtALMT12 represents an R-type anion channel required for stomatal movement in Arabidopsis guard cells.* Plant J, 2010. **63**(6): p. 1054-62.
46. Schulze, S., et al., *A Role for Calcium-Dependent Protein Kinases in Differential CO2- and ABA-Controlled Stomatal Closing and low CO2-induced Stomatal Opening in Arabidopsis.* New Phytol, 2021. **229**(5): p. 2765-2779.
47. Negi, J., et al., *CO2 regulator SLAC1 and its homologues are essential for anion homeostasis in plant cells.* Nature, 2008. **452**(7186): p. 483-6.
48. Jalakas, P., et al., *Combined action of guard cell plasma membrane rapid- and slow-type anion channels in stomatal regulation.* Plant Physiol, 2021. **187**(4): p. 2126-2133.
49. Ando, E., et al., *Elevated CO2 induces rapid dephosphorylation of plasma membrane H+-ATPase in guard cells.* New Phytologist, 2022. **236**(6): p. 2061-2074.
50. Hua, D., et al., *A plasma membrane receptor kinase, GHR1, mediates abscisic acid- and hydrogen peroxide-regulated stomatal movement in Arabidopsis.* Plant Cell, 2012. **24**(6): p. 2546-61.
51. Desikan, R., et al., *A new role for an old enzyme: nitrate reductase-mediated nitric oxide generation is required for abscisic acid-induced stomatal closure in Arabidopsis thaliana.* Proc Natl Acad Sci U S A, 2002. **99**(25): p. 16314-8.
52. Neill, S.J., et al., *Nitric Oxide Is a Novel Component of Abscisic Acid Signaling in Stomatal Guard Cells.* Plant Physiology, 2002. **128**(1): p. 13-16.
53. Joudoi, T., et al., *Nitrated cyclic GMP modulates guard cell signaling in Arabidopsis.* Plant Cell, 2013. **25**(2): p. 558-71.
54. Leckie, C.P., et al., *Abscisic acid-induced stomatal closure mediated by cyclic ADP-ribose.* Proc Natl Acad Sci U S A, 1998. **95**(26): p. 15837-42.
55. Zañudo, J.G. and R. Albert, *An effective network reduction approach to find the dynamical repertoire of discrete dynamic networks.* Chaos, 2013. **23**(2): p. 025111.
56. Deritei, D., et al., *Principles of dynamical modularity in biological regulatory networks.* Sci Rep, 2016. **6**: p. 21957.

bioRxiv preprint doi: https://doi.org/10.1101/2023.10.23.563079; this version posted October 25, 2023. The copyright holder for this preprint (which was not certified by peer review) is the author/funder, who has granted bioRxiv a license to display the preprint in perpetuity. It is made available under aCC-BY-NC 4.0 International license.

57. Wang, R.-S. and R. Albert, *Elementary signaling modes predict the essentiality of signal transduction network components.* BMC Systems Biology, 2011. **5**(1): p. 44.
58. Yang, G., J. Gómez Tejeda Zañudo, and R. Albert, *Target Control in Logical Models Using the Domain of Influence of Nodes.* Frontiers in Physiology, 2018. **9**.
59. Saadatpour, A., R. Albert, and T.C. Reluga, *A Reduction Method for Boolean Network Models Proven to Conserve Attractors.* SIAM Journal on Applied Dynamical Systems, 2013. **12**(4): p. 1997-2011.
60. Jeon, B.W., B.R. Acharya, and S.M. Assmann, *The Arabidopsis heterotrimeric G-protein β subunit, AGB1, is required for guard cell calcium sensing and calcium-induced calcium release.* The Plant Journal, 2019. **99**(2): p. 231-244.
61. Maheshwari, P., et al., *Model-driven discovery of calcium-related protein-phosphatase inhibition in plant guard cell signaling.* PLoS Comput Biol, 2019. **15**(10): p. e1007429.
62. Gayatri, G., S. Agurla, and A. Raghavendra, *Nitric oxide in guard cells as an important secondary messenger during stomatal closure.* Frontiers in Plant Science, 2013. **4**.
63. He, J., et al., *The BIG protein distinguishes the process of CO(2) -induced stomatal closure from the inhibition of stomatal opening by CO(2).* The New phytologist, 2018. **218**(1): p. 232-241.
64. Lee, M., et al., *The ABC transporter AtABCB14 is a malate importer and modulates stomatal response to CO2.* Nat Cell Biol, 2008. **10**(10): p. 1217-23.
65. Zhu, M., et al., *Preparation of Epidermal Peels and Guard Cell Protoplasts for Cellular, Electrophysiological, and -Omics Assays of Guard Cell Function*, in *Plant Signal Transduction: Methods and Protocols*, J.R. Botella and M.A. Botella, Editors. 2016, Springer New York: New York, NY. p. 89-121.
66. Wang, H., et al., *Elevated Carbon Dioxide Induces Stomatal Closure of Arabidopsis thaliana (L.) Heynh. Through an Increased Production of Nitric Oxide.* Journal of Plant Growth Regulation, 2015. **34**(2): p. 372-380.
67. Leung, J., S. Merlot, and J. Giraudat, *The Arabidopsis ABSCISIC ACID-INSENSITIVE2 (ABI2) and ABI1 genes encode homologous protein phosphatases 2C involved in abscisic acid signal transduction.* The Plant Cell, 1997. **9**(5): p. 759-771.
68. Sethi, J.K., R.M. Empson, and A. Galione, *Nicotinamide inhibits cyclic ADP-ribose-mediated calcium signalling in sea urchin eggs.* Biochem J, 1996. **319 (Pt 2)**: p. 613-7.
69. Walseth, T.F. and H.C. Lee, *Synthesis and characterization of antagonists of cyclic-ADP-ribose-induced Ca2+ release.* Biochim Biophys Acta, 1993. **1178**(3): p. 235-42.
70. Rakovic, S., et al., *An antagonist of cADP-ribose inhibits arrhythmogenic oscillations of intracellular Ca2+ in heart cells.* J Biol Chem, 1999. **274**(25): p. 17820-7.

bioRxiv preprint doi: https://doi.org/10.1101/2023.10.23.563079; this version posted October 25, 2023. The copyright holder for this preprint (which was not certified by peer review) is the author/funder, who has granted bioRxiv a license to display the preprint in perpetuity. It is made available under aCC-BY-NC 4.0 International license.

71. Nishimura, N., et al., *PYR/PYL/RCAR family members are major in-vivo ABI1 protein phosphatase 2C-interacting proteins in Arabidopsis.* Plant J, 2010. **61**(2): p. 290-9.
72. Umezawa, T., et al., *Type 2C protein phosphatases directly regulate abscisic acid-activated protein kinases in Arabidopsis.* Proc Natl Acad Sci U S A, 2009. **106**(41): p. 17588-93.
73. Vlad, F., et al., *Protein phosphatases 2C regulate the activation of the Snf1-related kinase OST1 by abscisic acid in Arabidopsis.* Plant Cell, 2009. **21**(10): p. 3170-84.
74. Geiger, D., et al., *Activity of guard cell anion channel SLAC1 is controlled by drought-stress signaling kinase-phosphatase pair.* Proc Natl Acad Sci U S A, 2009. **106**(50): p. 21425-30.
75. Scherzer, S., et al., *Multiple calcium-dependent kinases modulate ABA-activated guard cell anion channels.* Mol Plant, 2012. **5**(6): p. 1409-12.
76. Geiger, D., et al., *Guard cell anion channel SLAC1 is regulated by CDPK protein kinases with distinct Ca2+ affinities.* Proc Natl Acad Sci U S A, 2010. **107**(17): p. 8023-8.
77. Grondin, A., et al., *Aquaporins Contribute to ABA-Triggered Stomatal Closure through OST1-Mediated Phosphorylation.* Plant Cell, 2015. **27**(7): p. 1945-54.
78. Tõldsepp, K., et al., *Mitogen-activated protein kinases MPK4 and MPK12 are key components mediating CO.* Plant J, 2018. **96**(5): p. 1018-1035.
79. Sasaki, T., et al., *Closing plant stomata requires a homolog of an aluminum-activated malate transporter.* Plant Cell Physiol, 2010. **51**(3): p. 354-65.
80. Kinoshita, T., M. Nishimura, and K. Shimazaki, *Cytosolic Concentration of Ca2+ Regulates the Plasma Membrane H+-ATPase in Guard Cells of Fava Bean.* Plant Cell, 1995. **7**(8): p. 1333-1342.
81. Ward, J.M. and J.I. Schroeder, *Calcium-Activated K+ Channels and Calcium-Induced Calcium Release by Slow Vacuolar Ion Channels in Guard Cell Vacuoles Implicated in the Control of Stomatal Closure.* Plant Cell, 1994. **6**(5): p. 669-683.
82. Guse, A.H., *Cyclic ADP-ribose: a novel Ca2+-mobilising second messenger.* Cell Signal, 1999. **11**(5): p. 309-16.
83. Hayashi, M., et al., *Raf-like kinases CBC1 and CBC2 negatively regulate stomatal opening by negatively regulating plasma membrane H.* Photochem Photobiol Sci, 2020. **19**(1): p. 88-98.
84. Swatek, K.N., et al., *Multisite phosphorylation of 14-3-3 proteins by calcium-dependent protein kinases.* Biochem J, 2014. **459**(1): p. 15-25.
85. Brandt, B., et al., *Reconstitution of abscisic acid activation of SLAC1 anion channel by CPK6 and OST1 kinases and branched ABI1 PP2C phosphatase action.* Proc Natl Acad Sci U S A, 2012. **109**(26): p. 10593-8.
86. Mulaudzi, T., et al., *Identification of a novel Arabidopsis thaliana nitric oxide-binding molecule with guanylate cyclase activity in vitro.* FEBS Lett, 2011. **585**(17): p. 2693-7.

bioRxiv preprint doi: https://doi.org/10.1101/2023.10.23.563079; this version posted October 25, 2023. The copyright holder for this preprint (which was not certified by peer review) is the author/funder, who has granted bioRxiv a license to display the preprint in perpetuity. It is made available under aCC-BY-NC 4.0 International license.

87. Nagy, S.K., et al., *Activation of AtMPK9 through autophosphorylation that makes it independent of the canonical MAPK cascades.* Biochem J, 2015. **467**(1): p. 167-75.
88. Sokolovski, S. and M.R. Blatt, *Nitric oxide block of outward-rectifying K+ channels indicates direct control by protein nitrosylation in guard cells.* Plant Physiol, 2004. **136**(4): p. 4275-84.
89. Sirichandra, C., et al., *Phosphorylation of the Arabidopsis AtrbohF NADPH oxidase by OST1 protein kinase.* FEBS Lett, 2009. **583**(18): p. 2982-6.
90. Acharya, B.R., et al., *Open Stomata 1 (OST1) is limiting in abscisic acid responses of Arabidopsis guard cells.* New Phytol, 2013. **200**(4): p. 1049-63.
91. Imes, D., et al., *Open stomata 1 (OST1) kinase controls R-type anion channel QUAC1 in Arabidopsis guard cells.* Plant J, 2013. **74**(3): p. 372-82.
92. Meinhard, M. and E. Grill, *Hydrogen peroxide is a regulator of ABI1, a protein phosphatase 2C from Arabidopsis.* FEBS Lett, 2001. **508**(3): p. 443-6.
93. Meinhard, M., P.L. Rodriguez, and E. Grill, *The sensitivity of ABI2 to hydrogen peroxide links the abscisic acid-response regulator to redox signalling.* Planta, 2002. **214**(5): p. 775-82.
94. Sridharamurthy, M., et al., *H2O2 inhibits ABA-signaling protein phosphatase HAB1.* PLoS One, 2014. **9**(12): p. e113643.
95. Bright, J., et al., *ABA-induced NO generation and stomatal closure in Arabidopsis are dependent on H2O2 synthesis.* Plant J, 2006. **45**(1): p. 113-22.
96. Zhang, X., et al., *Inhibition of blue light-dependent H+ pumping by abscisic acid through hydrogen peroxide-induced dephosphorylation of the plasma membrane H+-ATPase in guard cell protoplasts.* Plant Physiol, 2004. **136**(4): p. 4150-8.
97. Kohler, B., A. Hills, and M.R. Blatt, *Control of guard cell ion channels by hydrogen peroxide and abscisic acid indicates their action through alternate signaling pathways.* Plant Physiol, 2003. **131**(2): p. 385-8.

bioRxiv preprint doi: https://doi.org/10.1101/2023.10.23.563079; this version posted October 25, 2023. The copyright holder for this preprint (which was not certified by peer review) is the author/funder, who has granted bioRxiv a license to display the preprint in perpetuity. It is made available under aCC-BY-NC 4.0 International license.

Start node	End node	Type	Ref.
8-nitro-cGMP	ADPRc	+, A	[68-70]
ABI1	OST1 minimum function	-, D	[71-73]
ABI1	OST1 activated	-, D	[71-73]
ABI1	SLAC1 generic	-, I	[74-76]
ABI1	SLAC1 CO_2	-, I	[74-76]
ABI2	OST1 minimum function	-, D	[73]
ABI2	OST1 activated	-, D	[73]
ABI2	GHR1	-, D	[50]
ABI2	SLAC1 generic	-, I	[74-76]
ABI2	SLAC1 CO_2	-, I	[74-76]
ADPRc	cADPR	+, D	
AnionEM	Depolarization	+, D	
AnionEM	H_2O Efflux	+, D	
Aquaporins	H_2O Efflux	+, D	[6, 77]
Ca^{2+} ATPase	Ca^{2+}_{cyt}	-, D	
CA1/4	HCO_3^-	+, D	[7, 8]
CA1/4	RHC1	+, D	[15]
Ca^{2+}_{cyt}	MPK activity	+, I	[11, 35, 78]
Ca^{2+}_{cyt}	Ca^{2+} ATPase	+, D	[23]
Ca^{2+}_{cyt}	CPKs	+, D	[75]
Ca^{2+}_{cyt}	QUAC1	+, A	[79]
Ca^{2+}_{cyt}	H^+ ATPase	-, D	[80]
Ca^{2+}_{cyt}	KEV	+, D	[81]
Ca^{2+}_{cyt}	Depolarization	+, D	
cADPR	CIS	+, I	[82]
CaIM	ABI1	-, I	[61]
CaIM	ABI2	-, I	[61]
CaIM	HAB1	-, I	[61]
CaIM	Ca^{2+}_{cyt}	+, D	
CBC1/2	SLAC1 CO_2	-	[83]
cGMP	8-nitro-cGMP	+, D	
CIS	Ca^{2+}_{cyt}	+, D	
CO_2 entry of cell	HCO_3^-	+, D	[7, 8]
CO_2 porins	CO_2 entry of cell	+, D	[6]
CPKs	CPKs	+, D/A	[84]
CPKs	SLAC1 generic	+, D	[75, 76, 85]
Depolarization	KOUT	+, D	
GHR1	CaIM	+, A	[50]
GHR1	CPKs	+, D	[41]
GHR1	SLAC1 generic	-, D	[50]
GHR1	SLAC1 CO_2	-, D	[50]
GTP	cGMP	+, D	[86]
H^+ ATPase	Depolarization	-, D	
H_2O Efflux	Closure	+, D	
HAB1	OST1 minimum function	-, D	[73]
HAB1	OST1 activated	-, D	[73]
HCO_3^-	MPKs-HT1 complex	+, D	[11-14, 16]
HCO_3^-	RHC1	+, D	[15]
HCO_3^-	SLAC1 CO_2	+, A	[36]
High CO_2	CO_2 entry of cell	+, D	
HT1	CBC1/2	+, D	[13]
HT1	GHR1	-, D	[11, 15]
HT1	OST1 minimum function	-, D	[11, 15]
HT1	OST1 activated	-, D	[11, 15]
K^+ efflux	Depolarization	-, D	
K^+ efflux	H_2O Efflux	+, D	
K^+ efflux	K^+ efflux	+, A	
KEV	Depolarization	+, D	
KEV	K^+ efflux	+, D	
KOUT	K^+ efflux	+, D	
MPKs	MPKs-HT1 complex	+, D	
MPKs	MPK activity	+, D	
MPKs-HT1 complex	HT1	-, D	[11-14]
MPK activity	HT1	-, A	[11, 16, 35]
MPK activity	MPK activity	+, D/A	[87]
MPK activity	SLAC1 generic	+, A	[35]
NAD^+	cADPR	+, D	
NADPH	NO	+, D	[51]
NADPH	ROS	+, D	
NIA1/2	NO	+, D	[51]
Nitrite	NO	+, D	[51]
NO	8-nitro-cGMP	+, I	[53]
NO	NOGC	+, D	[86]
NO	KOUT	-, I	[88]
NOGC	cGMP	+, D	[86]
OST1 activated	SLAC1 generic	+, D	[74]
OST1 minimum function	OST1 activated	+, D	
OST1 minimum function	RbohD/F	+, D	[89]
OST1 minimum function	SLAC1 generic	+, D	[74, 90]
OST1 minimum function	SLAC1 CO_2	+, D	[74, 90]
OST1 minimum function	QUAC1	+, D	[91]
OST1 minimum function	Aquaporins	+, D	[77]
QUAC1	AnionEM	+, D	[45]
RbohD/F	ROS	+, D	
RHC1	HT1	-, D	[15]
ROS	GHR1	+, I	[50]
ROS	ABI1	-, D	[92]
ROS	ABI2	-, D	[93]
ROS	HAB1	-, D	[94]
ROS	8-nitro-cGMP	+, I	[53]
ROS	NIA1/2	+, A	[95]
ROS	H^+ ATPase	-, D	[96]
ROS	KOUT	-, I	[97]
SLAC1 CO_2	AnionEM	+, D	
SLAC1 nonCO_2	AnionEM	+, D	

Table 1. Edge list of the high CO_2 induced closure network

The edges represent interactions and regulatory effects. The start node (first column) indicates the source of the interaction and the end node (second column) indicates the target of the interaction. "Type" records the sign and type of the edge. Positive edge sign, "+", indicates positive/activating regulation and "–" indicates negative/inhibitory regulation. For edge type, we use "D" for direct regulation, "I" for indirect regulation, and "A" for assumed regulation. In rare cases we use "D/A" to represent an edge that is supported by a direct interaction but has assumed properties, e.g. assumed direction or sign. "Ref." column records the reference that supports the edge ("P" is short for "Palani's preprint"). Edges representing known biophysical/biochemical processes, e.g. AnionEM → Depolarization, do not have a reference. The table follows alphabetic order of the start node.